Original Article

Şakir Altınsoy*, Selen Erkan, Nuray Beköz Üllen, Sezen Canım Ateş and Neşe Evcil

Evaluation of surface properties of modified Ti6Al4V alloy with copper nanoparticles organic nanostructure for biomedical applications: dependency on anticorrosive, antibacterial, and biocompatibility

https://doi.org/10.1515/corrrev-2023-0148
Received November 18, 2023; accepted August 20, 2024;
published online November 12, 2024

Abstract: In this study, a novel multifunctional copper nanoparticle CuNPs in the organic biomatrix was coated to the surface of Ti6Al4V to create multifunctional features. The synthesis of CuNPs was carried out by plant-mediated green synthesis method obtained from *Moringa* leaf extract, and the prepared CuNPs were coated on the substrate surfaces as single and double layers with drop casting methods. Characterizations of the synthesized CuNPs were performed by UV–Vis, FTIR, XRD, and SEM methods. Characterization of the modified Ti6Al4V alloy surfaces was performed using SEM-EDS and surface roughness analysis. The electrochemical corrosion, antibacterial behavior, and cytotoxic effects of coated and noncoated Ti6Al4V as a function of biocompatibility properties were also tested. The synthesized CuNPs have a homogeneously dispersed spherical shape. Biocorrosion tests have clearly demonstrated that the coating forms a protective film on the substrate surface, and the resistance increased by 49 %. Antibacterial results show that the single and double-coated Ti6Al4V alloy samples with CuNPs organic nanostructure had improved biocompatibility. However, it was determined that the cytotoxic effect increases proportionally with the coating. The obtained results show the importance of surface modification in the appropriate nanostructure to obtain multifunctional nanoplatforms that show promise in biomedical applications.

Keywords: Ti6Al4V; nanoparticles; biocorrosion; antibacterial; biocompatibility

***Corresponding author: Şakir Altınsoy**, Department of Biomedical Engineering, Faculty of Engineering and Architecture, Istanbul Yeni Yüzyıl University, Istanbul 34010, Türkiye, E-mail: sakir.altinsoy@yeniyuzyil.edu.tr. https://orcid.org/0000-0002-1893-2266
Selen Erkan, Department of Biomedical Engineering, Institute of Science and Technology, Istanbul Yeni Yüzyıl University, Istanbul 34010, Türkiye
Nuray Beköz Üllen, Department of Metallurgical and Materials Engineering, Faculty of Engineering, Istanbul University-Cerrahpaşa, Istanbul 34320, Türkiye
Sezen Canım Ateş, Department of Biomedical Engineering, Faculty of Engineering and Architecture, Istanbul Yeni Yüzyıl University, Istanbul 34010, Türkiye
Neşe Evcil, Department of Bioengineering, Institute of Science and Technology, Yıldız Technical University, Istanbul 34220, Türkiye

1 Introduction

Nanomaterials provide advantages in fields such as medication, water treatment systems, solar energy conversion, and catalysis (Benakashani et al. 2016; Ullah 2022a,b). Nanomaterials play a significant role in the fields of biology and medicine due to their metallic nanoparticles and attractive physicochemical properties. In the recent years, the interest of researchers in herbal essences in the synthesis of biogenic nanoparticles has increased. The primary cause of this is that the herbal essences are inexpensive, suitable for serial production, not requiring special protection conditions, don't bear the risk of contamination, and are very stable under compelling conditions (such as high temperature, extensive pH range, and salt) (Duman et al. 2016). For the synthesis of nanoparticles, there are numerous synthesizing methods such as the use of microwave, thermal decomposition, and green chemistry methods (Begum et al. 2009; Navaladian et al. 2007; Sreeram et al. 2008; Starowicz et al. 2006). For the synthesis of copper nanoparticles, the development of a reliable green synthesis process is very meaningful in nanotechnology research. Compared with the physical and chemical methods, green synthesis has many advantages: environment-friendly, cost-effective, and easily scalable for the large scaled synthesis. As the materials inclusive of metal particles in nanometer size may exhibit unique properties such as optic, electronic,

magnetic etc., they have drawn high attention in recent years (Soloviev and Gedanken 2011). It has been accepted that many properties of the materials don't just depend on their chemical compositions but also on the particle size, shape, and structure. Many studies in recent years have stated that silver and copper nanoparticles are coated on different materials (Gong et al. 2007; Irzh et al. 2007; Perelshtein et al. 2008).

Various metallic substrate materials such as titanium (Ti), Ti alloys, and stainless steel are extensively used in screw implants in medical equipment, surgical tool constructs, and dental constructs (Alias et al. 2019; Raza et al. 2016). Titanium and its alloys are extensively used in many medical applications as orthopedics and dentistry being in the first place due to their corrosion resistance, mechanical properties, high biocompatibility, and nontoxicity (Chen and Thouas 2015; Cui et al. 2023; E. Zhang et al. 2021; Gnanavel et al. 2018; Li et al. 2020; Quinn et al. 2020; Święch et al. 2023; Xi and Wong 2021). Pure titanium (grade 1 to 4, α structure) and commercial TiV (Ti6Al4V, Ti6Al4V ELI) alloys are the ones that are used the most in implant applications (El hadad et al. 2020; Mierzejewska et al. 2019; Prestat and Thierry 2021; Shokrani et al. 2016; Vu et al. 2016; Yağmur and Pul 2021; Zhang and Chen 2019). The excellent corrosion resistance of Ti and its alloys is due to the formation of a protective passive oxide (TiO_2) layer on its surface in many environments (Rahimi et al. 2021; Xavier 2020). However, the passive oxide film layer can be damaged by mechanical damage in the presence of body fluid containing inorganic (i.e., electrolytes Na^+, K^+, Cl^-, PO_4^{3-}) and organic (i.e., plasma proteins) compounds. This situation can cause many undesirable effects on the human body. With the acceleration of the corrosion process, toxicity increases and causes inflammation (Asri et al. 2017; Bocchetta et al. 2021; Pan et al. 1997; Święch et al. 2023). Titanium is extensively used in clinical terms because infection due to implants is still one of the most significant complications. The treatment of this infection is generally difficult, and it sometimes causes the removal of the implant and repeated surgeries (Zhao et al. 2009, 2011). Despite the materials produced by different manufacturing methods having the same surface roughness, in some cases, their characterization properties such as friction, corrosion, and fatigue strength may differ. In the improvement and determination of the surface quality of materials to be produced, the measurement of surface roughness is very important. The increase in surface quality is ensured through the decrease in roughness value, and this is possible by the coating methods. A case on the contrary causes unnecessary cost increase and time loss (Shokrani et al. 2016).

The modification of Ti alloy surface may be a good way the improvement of biocompatibility and osseointegration (Chen et al. 2021; Zhang et al. 2015) as well as antibacterial (Freitas et al. 2021; Liu et al. 2020; Van Hengel et al. 2020; Xia et al. 2020), antimicrobial (Calabrese et al. 2022), and corrosion (Xia et al. 2020) properties. The significance of biomaterials containing Cu gradually increases, which causes researchers to conduct more studies on this type of material (Wang et al. 2021). Currently used methods of obtaining Cu-containing materials can be divided into some groups: addition of Cu to the molten metal (Ren et al. 2015), accumulation of a Cu coating on the metallic surface (Huang et al. 2018; Zhao et al. 2019), and Cu nanoparticles (Xia et al. 2020). Liu et al. (Liu et al. 2020) reported that the medical application of CuNPs and modification of metallic surfaces ensures good corrosion resistance and improved mechanical properties of the modified surfaces. Many researchers have indicated that the improvement of the biological and physicochemical properties of the metallic surface may be associated with modification with CuNPs (Calabrese et al. 2022; Freitas et al. 2021; Liu et al. 2020; Lu et al. 2021; Van Hengel et al. 2020; Xia et al. 2020). The high surface area/volume rate of NPs may cause the amplification of oxidation on the small-sized implant surface, and it may cause the release of metallic ions, which may cause antibacterial effects (Van Hengel et al. 2020). Cu is an element that is important in the human body and causes many functions in physiological activities. It provides antibacterial and antimicrobial properties and plays an active role in angiogenesis (Cai et al. 2019; E. Zhang et al. 2021; Święch et al. 2023; Xie and Kang 2009; Xia et al. 2020). The surface treatment of medical devices being coated with antibacterial materials is a promising solution. Today, copper, silver, and their compounds are the most extensively used antibacterial materials due to their strong, wide-spectrum antimicrobial effects against bacteria, fungi, and viruses (Cai et al. 2019). Especially plant-mediated CuNPs are preferred for biomedical uses because they are biocompatible and produced by the green methods (Freitas et al. 2021; Liu et al. 2020). According to some studies, the fruits, seeds, and leaves of the *Moringa oleifera* plant are used to purify turbid water. *M. oleifera* leaves contain cationic polyelectrolytes. It has many advantages such as economical production, low sludge volume, rapid decomposition of sludge, and unaffected PH of water. In addition, *M. oleifera* leaves have antimicrobial properties and contain various proteins, lignin components, fatty acids, and carbohydrates. Metabolizable energy and organic matter digestibility estimated from the extent of fermentation in *in vitro* incubation are available for extracted and unextracted leaves (Suresh and Balamurugan 2021). In the present study, the synthesis of CuNPs was carried out using *Moringa leaf* extract by the green synthesis method (Surendhiran et al. 2021), synthesized CuONPs by green synthesis method using *M. oleifera* leaf extract as reducing and sealing agents, and investigated the photocatalytic activity and anticorrosive behavior of CuONPs. They

Table 1: Studies on the coating of various metallic materials with metallic nanoparticles.

Reference	Substrate	Coating material	Coating method	Characterization studies
Święch et al. (2023)	Ti	CuNps	Deposition	Structure characterization (SEM), electrochemical, UV–Vis, FTIR and SEIRA, Raman and SERS, nano-SEIRA measurements
Roguska et al. (2011)	Pure Ti	TiO_2, Ag, Au, Cu–Nps	Sputter deposition	Structure characterization (SEM), microanalytical (AES) methods, SERS measurements
Zhao et al. (2019)	Pure Ti	(Mg–Cu–F)	Micro-arc oxidation (MAO)	Coating characterization (SEM), cell morphology, antibacterial activity, osteogenic activity
Xia et al. (2020)	Pure Ti	C/Cu	Plasma immersion ion implantation and deposition technology	Surface characterization (SEM), electrochemical performance, hardness of surface, antibacterial ability, cytotoxicity evaluation
Soloviev and Gedanken (2011)	304 stainless steel plate	$AgNO_3$–Nps	Sonochemical	Structure characterization SEM, XRD, DRS
Chou et al. (2005)	Cellulose acetate	$AgNO_3$–Nps	Spinning	Surface characterization (SEM), anti-bacteria test, halo test
Gil et al. (2006)	Undoped lead crystal glass	$AgNO_3$–Nps	Sol–gel	Ion-exchange, TEM, SEM
Jin et al. (2014)	Pure Ti	Zn ion implantation	Plasma immersion ion implantation technology	Surface chemistry and structure characterization, *in vitro* cytocompatibility evaluation, antibacterial test
Bai et al. (2019)	Ti6Al4V	TiSiN/Cu nano	Multi-arc ion plating	Microstructure characterization (SEM-EDX), XRD, antibacterial testing, hardness and elastic modulus, antifouling test
Cheng et al. (2010)	440a stainless steel	Nanocomposite TiSiN	Large area filtered arc deposition (LAFAD) technique	Mechanical properties and tribological behaviors
Shan et al. (2016)	316L	CrN and CrSiN	Multi-arc ion plating	Structure characterization, tribological (corrosion and wear behaviors)
Gnanavel et al. (2018)	Titanium alloy (Ti–6Al–4V) and 316L stainless-steel	Hydroxyapatite (HAP) ceramics	Pulsed laser deposition technique	Morphology analysis SEM- EDS, XRD, AFM, electrochemical measurements
Fernández-Arias et al. (2020)	Cp-Ti (commercial pure-Ti)	CuNPs coating	Laser ablation	Physicochemical characterization of the film, characterization of the obtained nanoparticles, XRD, antimicrobial activity
Yu et al. (2016)	Cp-Ti	CuNPs coating	Plasma immersion ion implantation and deposition	Surface characterization (SEM-EDX), wettability, electrochemical corrosion, antimicrobial activity
He et al. (2017)	Cp-Ti	CuO–TiO_2 coating	Magnetron sputtering	Microstructure and phase analysis (SEM-EDX), XRD, cytocompatibility evaluation, electrochemical corrosion, antibacterial evaluation
Hadidi et al. (2017)	Ti6Al4V	3Cu–HA coating, 5Cu–HA coating	Electrophoretic deposition	SEM-EDX, XRD, antimicrobial activity test, cell culture and MTT assay, statistical analysis.
Hidalgo-Robatto et al. (2018)	Ti6Al4V	2.5Cu–HA coating	Laser deposition	Sample characterization (FTIR, SEM-EDX, XRD), biological characterization, biological activity
Zong et al. (2017)	Cp-Ti	Cu–Ti–O NTAs	Anodizing magnetron-sputtered	Sample characterization, antibacterial activity, cell adhesion, cytotoxicity, and proliferation
This study	Ti6Al4V	CuNPs coating	Dropping	Surface roughness, (FTIR, SEM-EDX, XRD), biocorrosion, antibacterial, biocompatibility

reported that CuONPs prepared according to the results are potentially suitable candidates for multifunctional applications. A summary of scientific studies on the characterization processes applied to metal-based NPs coated on the surface of different metal-based substrates are reported in Table 1. One of the most important steps for the industrial development of innovative and multifunctional coatings is the development of nanometal-based surfaces. The aim of this study is to create a guide in this field. The present study is the first effort done to green synthesize of CuNPs in the organic biomatrix from the extract of *Moringa* leaf. This study and the characterization studies were made to contribute to the development of nanotechnology toward a green approach. This study was intended to improve the surface properties and biocorrosion resistance of Ti6Al4V alloy pieces being coated with different thicknesses by the synthesized CuNPs using *Moringa* leaf extract. Moreover, the antibacterial and cytotoxic tests were performed, and an examination was made regarding its possible effects on the body during implementation. It is believed that optimizing the process parameters in nanocoating will yield efficient results and open new avenues in the medical applications of Ti-based implants. Moreover, the proposed approach would also open up new routes to explore green metal-based NPs coated on biometals in biomedical applications.

2 Materials and methods

2.1 Materials

Ti6Al4V alloy rods with ASTM standard number B348 and with a diameter of 30 mm obtained from Varzene Metal Industry and Trade Inc. was used as the substrate material. The chemical composition of Ti6Al4V alloy is given in Table 2. Orthogonal surface turning machined of Ti6Al4V alloy specimens was performed on a CNC (computer numerical control) lathe center having a variable spindle speed of 3,000 rpm rated at 30 kW, produced by YouJi Machine Industrial Co. Ltd. (Taiwan). In all surface turning operations, the water-based lubricant was used as cutting fluid. The specimens were prepared in dimensions of Ø25 × 2.5 mm with a cutting speed of 30 m/min, feed rate of 0.15 mm/dev, and cutting depths of 0.6 mm.

M. oleifera leaves, copper (II) sulfate pentahydrate salt ($CuSO_4.5H_2O$ 99 % purity and molar mass: 249.68 g/mol), sodium hydroxide (NaOH), ethanol, and distilled water were used for the synthesis of CuNPs in the organic biomatrix. All chemical-based compounds are analytical-based reagents from Merck Company (Germany) and Sigma Aldrich Company (Germany).

Table 2: Chemical composition of Ti6Al4V alloy (wt.%).

Element	Al	V	Fe	C	N	H	O	Ti
Ti6Al4V	6.09	3.9	0.13	0.02	0.01	0.001	0.09	Bal.

2.2 Preparation of *Moringa* leaf extract

To prepare the extract, dust on the surface of *Moringa* leaves was removed by washing with distilled water. The cleaned leaves were dried at room condition for 3 days. After drying, the leaves were ground and sieved to powder. 10 gr/250 mL distilled water was added to the sifted fine *Moringa* powders and then boiled at 50 °C for 1 h. The resulting solution was cooled at room temperature and kept in the dark for 3 days. Then, the resulting solution to obtain *Moringa* extract was filtered using a sterile syringe filter and stored in sterile glass containers until used at 25 °C.

2.3 Preparation of *Moringa* extract-based CuNPs

Green synthesized CuNPs in the organic biomatrix was synthesized by an ultrasound sonication method using *Moringa* leaf extract. Firstly, *Moringa* extract was added to 0.1 M $CuSO_4.5H_2O$ (4:1 v/v) and heated to 90 °C with continuous stirring for 60 min. The stirred solution was kept in a dark place for 24 h and sonicated for 30 min at 45 % amplitude frequency at 25 °C. The separated precipitate was washed with distilled water and ethanol to remove the remaining organic-based extract and then dried in an oven at 100 °C for 1 h. After all these procedures, 1 mL of NaOH solution was added dropwise to the extract solution. The last samples were filtered with a sterile syringe filter. It was stored in a sterile glass container in a vacuum desiccator at 25 °C until the time of use.

2.4 Coating of Ti6Al4V with CuNPs

The synthesized CuNPs organic nanostructure was coated on Ti6Al4V substrate with the drop-casting method. Before starting the coating process in order to obtain cleaner surfaces, the Ti6Al4V discs were kept in ethanol in P select a brand ultrasonic bath device of Ultrasons HD model (Spain) for 15 min and then dried in an oven at 75 °C for 15 min. Eight drops with a value of 0.4 mL were applied using Pasteur pipette 3 mL on the cleaned Ti6Al4V discs. The coated substrate specimens were subjected to drying operation for 1 h at 60 °C using Binder GmbH Company (Germany) a drying-oven device. The coating operation was repeated under the same conditions for the double-coated

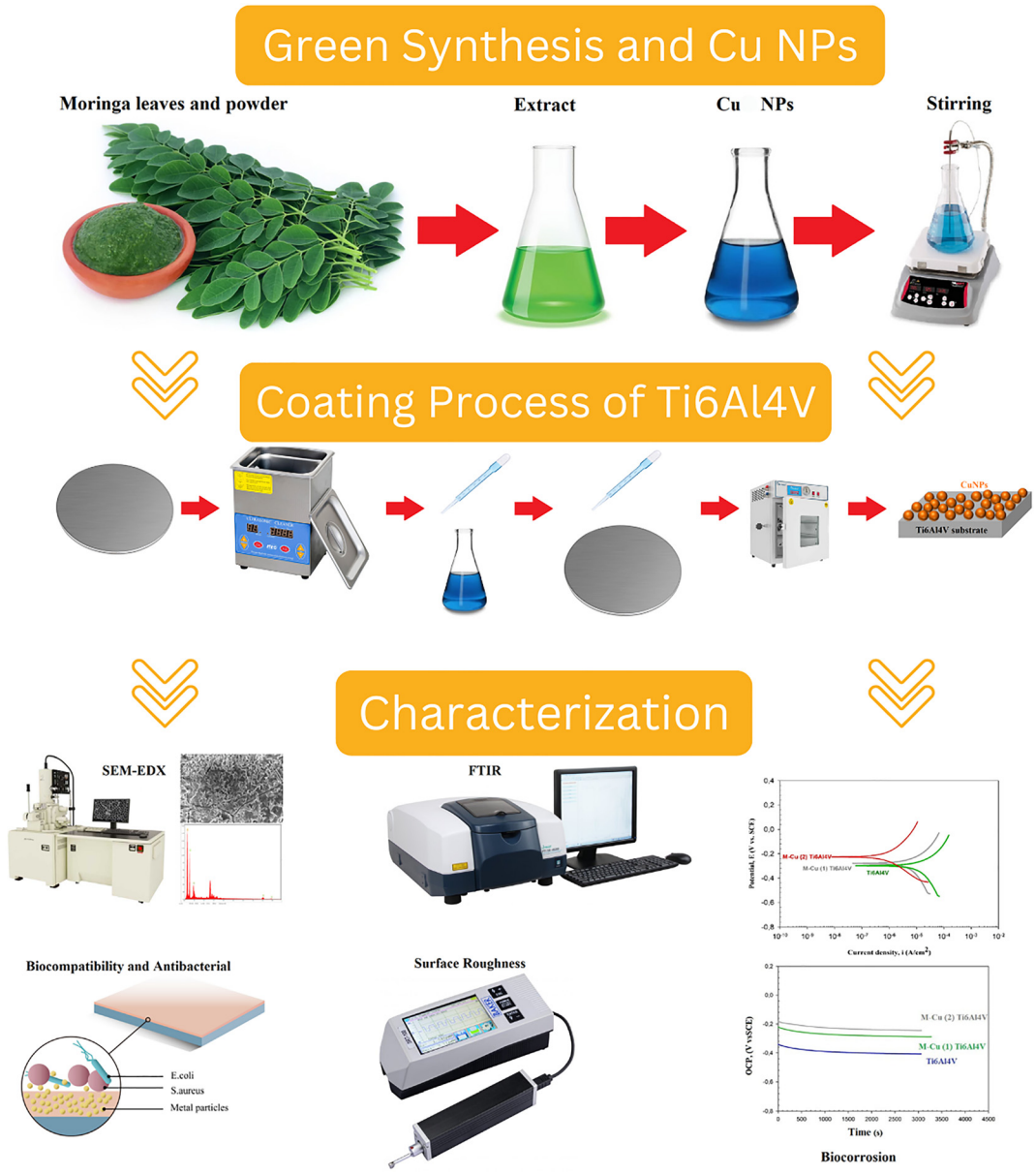

Figure 1: Schematic view of the synthesis, the coating, and the characterization steps.

specimens. The schematic view of the green method synthesis, nanocoating process, and characterization stages is given in Figure 1.

2.5 Characterization studies

2.5.1 Characterization of materials

In this study, ultraviolet visible spectrophotometry (UV–Vis) (UV-1900i model-Thailand), Fourier transform infrared (FTIR) spectroscopy, X-ray diffraction (XRD), and scanning electron microscopy (SEM-EDS) were used to characterize the synthesized CuNPs organic nanostructure. The absorbances of the synthesized CuNPs were determined by UV–Vis spectrophotometer with UV-Win 5 Software. For the FTIR analysis was performed up to the value of 4,000 cm^{-1} using a 70v brand (Vertex Company-United States) FTIR spectrophotometer. In the XRD analyses, the PANaltyticalEmpyrean brand device (United Kingdom) was used on a sample of 5 kV/40 mA with a scanning rate of 4°/min and an angle range of 2θ–θ, 10–90°. For the SEM-EDS analysis was used a Zeiss-Sigma 300 model (Germany) device. The morphology of the surface-modified Ti6Al4V samples was characterized by SEM/EDS. Surface roughness values of noncoated specimens and CuNPs-coated Ti6Al4V specimens were measured with

the Surftest 210 type Mitutoyo surface profilometer (Mitutoyo, Japan). In this study, the surfaces of four pieces were coated for each coating layer. The samples coated with the drop-casting method were averaged by performing three measurements from the different points of each surface. Thus, the surface roughness measurements of the surfaces coated with different coating thicknesses were made.

2.5.2 Electrochemical corrosion tests

Electrochemical corrosion tests were performed in body fluid solution using a computer-controlled potentiostat (Interface 1,000 Potentiostat, Gamry, USA). The volume of the corrosion test cell made of glass is 1,000 mL. The study was carried out in a conventional three-electrode system with high-density graphite as the counter electrode, a saturated calomel electrode (SCE) as the reference electrode, and a sample as the working electrode. Data analyses were determined by computer software (Framework and Echem Analyst Gamry). The noncoated and surface-modified Ti6Al4V samples were prepared by cutting and then mounting into an epoxy resin. The samples were connected to the system with a copper wire. Experiments were carried out at room temperature. The OCP value of the samples was measured before starting the electrochemical corrosion experiments. OCP level measurements were performed for 2 and 3 h until the OCP value stabilized. Since the OCP curve has an asymptotically stable region, the OCP value was considered stable. Tafel curves were determined by polarizing the samples with respect to OCP between −250 mV and +250 mV at a scanning rate of 1.0 mV/s. The samples coated with the drop-casting method were averaged by performing three measurements for every sample. In order to verify the test results, all electrochemical tests were performed on three samples under the same conditions. Graphical calculations were made by taking the arithmetic average of the measurement results.

2.5.3 Antibacterial activity tests

Since the CuNPs-coated Ti6Al4V samples are considered for use as biomaterials, antibacterial and cytotoxic tests were performed, and their possible effects on the body or during implantation were analyzed. *Staphylococcus aureus* (*S. aureus*) ATCC: 25,923 and *Escherichia coli* (*E. coli*) ATCC: 25,923 strains obtained from Yıldız Technical University Molecular Biology and Genetics Department were used in the antibacterial activity tests of this study (ATCC: American Type Culture Collection). Both strains were allowed to grow overnight in an incubator on Mueller-Hinton Broth (MHB) at 37 °C with shaking at 200 rpm. Bacterial cultures were diluted with sterile MHB until the optical density was adjusted from 0.1 to 0.2 at 600 nm (corresponding to 108 CFU/mL). This concentration was used for the colony counting method according to the literature to evaluate the antibacterial properties of material samples against Gram-positive *S. aureus* and Gram-negative *E. coli* bacteria (Süer et al. 2021). Briefly, all samples were sterilized by autoclaving at 121 °C for 20 min before the experiments, and the antibacterial study was carried out in a sterile environment. About 10 µL of the prepared *S. aureus* and *E. coli* bacteria solutions were taken and inoculated by dropping separately on the surfaces of the noncoated, single-coated, and double-coated material samples. These materials were incubated at 37 °C and greater than 90 % relative humidity for 1 h. Then, the material samples were transferred to sterile containers containing 10 mL of MHB medium to recover the viable microorganisms. Containers of the material samples were kept at room temperature for 30 min and 10-fold serial dilutions were made. Samples of 100 µL were taken from each dilution and spread on MHA agar petri dishes with a drigalski-spatula. Petri dishes were incubated at 37 °C for 24 h and then colony counted, defined as colony forming units per mL (cfu/mL). The % kill was calculated with the following Equation (1).

$$\%\text{Killing} = \frac{\text{Colony count of control} - \text{Colony count of test samples}}{\text{Colony count of control}} \times 100 \quad (1)$$

2.5.4 Cytotoxic tests

Cytotoxicity is a measure of the potential of a sample to cause cell injury (Shaw 1994). The most common of cytotoxicity assay, the Thiazolyl Blue Tetrazolium Bromide (MTT) assay, is a colorimetric cytotoxicity assay based on measuring the metabolic activity levels of cell mitochondria (Hussain et al. 1993). The principle of the MTT method is based on the mitochondrial dehydrogenase enzyme found in the mitochondria of living cells oxidizes lactate to pyruvate, while the $NADH^+$ released turns the yellow MTT reactant into purple formazan crystals. Formed purple formazan crystals are directly proportional to active metabolism and cell viability (Van Meerloo et al. 2011). For biocompatibility evaluation, sterile single-coated, double-coated, and noncoated specimens were incubated at 37 °C for 7 days by adding 5 mL of DMEM F12 medium. All the specimens were taken from the

medium interacting with the metals on the 1st, 4th, and 7th days and stored at +4 °C (Köse et al. 2018). L929 cells taken from the nitrogen tank were dissolved in water at 37 °C. Cells were transferred to 4 mL of DMEM F12 medium with 10 % FBS and centrifuged at 1,000 rpm for 5 min. After centrifugation, the supernatants were removed. Cells were transferred to a 25 cm^2 flask with 5 mL of DMEM F12 medium with 10 % FBS. When the cells covered 90 % of the flask, the medium was removed from the flask, and 1 mL of trypsin-EDTA solution was added and incubated for 5 min. After it was observed that the cells were separated from the surface, the cells were transferred to the centrifuge tube with 2 mL of medium. The cells were centrifuged at 1,000 rpm for 5 min, and the supernatants were removed. The cell pellet that settled to the bottom after centrifugation was completed to 1 mL with the medium and counted with the help of trypan blue (Acar Derman et al. 2017).

After counting, cells were seeded into a 96-well microplate with a final volume of 100 µL at 10,000 cells/well. At the end of the 24 h incubation, it was observed that the cells covered the wells, and the entire medium was removed, and 100 µL of the 1st, 4th, and 7th day samples were added to the wells. This was done in eight repetitions. Cells were incubated with samples for 24 h. At the 24th hour of incubation, 10 µL of sterile MTT solution (10 mg/mL) was added to each of the wells and incubated for 4 h in the dark. To dissolve the formazan crystals formed at the end of this period, 100 µL of DMSO was added to each of the wells and incubated for another 30 min. Afterward, the absorbance values in the wells were determined by reading the microplate in an ELISA plate reader at a wavelength of 540 nm. Finally, the viability of the cells was calculated from these absorbance values with the following Equation (2) (Köse et al. 2018; Mansuroğlu et al. 2020).

$$\%\,\text{Cell viability} = \frac{0D_{540}\,(\text{sample})}{0D_{540}\,(\text{control})}\,x\,100 \qquad (2)$$

3 Results and discussion

3.1 Characterization of the *Moringa* extract-based CuNPs

The UV–Vis measurement was performed to study surface plasmon resonance (SPR) of synthesized CuNPs in the organic biomatrix. SPR consists of the absorption of visible electromagnetic energy as a result of the combined fluctuation of electron transfer on the surface of CuNPs (Punniyakotti et al. 2020). The reduction of the extract was confirmed by the absorptivity at 550 nm observed in the UV–Vis spectroscopy

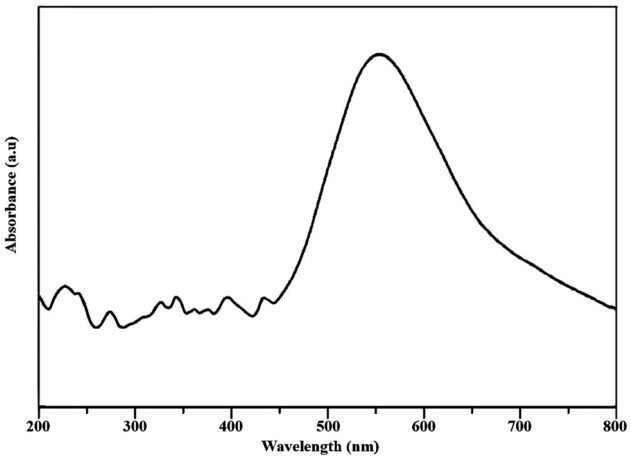

Figure 2: UV–Vis spectrum of synthesized CuNPs using *Moringa* leaf extract.

record. CuNPs exhibited a broad peak between 500 nm and 600 nm, with the peak at 550 nm. Figure 2 shows the highest absorbance at approximately 550 nm confirming the formation of CuNPs. This absorbance band appears typical for CuNPs. The width of the bands belonging to NPs is an indicator that the particles exhibit polydispersion, that is, a polydisperse distribution. SPR behavior varies depending on the shape, size, distribution, and matrix structures of NPs. The reason why different maximum absorbance bands are obtained in UV–Vis results in studies in the literature is that NPs vary according to their shape, size, distribution status, and matrix structures. SPR peak values between 500 and 600 nm have been reported by many researchers for CuNPs synthesized using a green reducing agent (Nasrollahzadeh et al. 2017; Rajesh et al. 2018).

The functional groups of *Moringa* extract-based CuNPs used in this study were performed using FTIR analysis. The FTIR spectrum of CuNPs, given in Figure 3, shows the interaction between CuSO4.5H2O and the relevant regions for the production of phytochemicals, illustrative differences in the shape and position of the signals. The bands clearly seen in the figure are lattice vibration modes indicating the functional groups of biomolecules absorbed on the nanoparticles. The sharp absorption peaks were observed in the range of 1,600–600 cm^{-1}. FTIR spectra of CuNPs showed vibrations in the region of 640–1,595 cm^{-1}, which can be attributed to Cu vibrations confirming the formation of CuNPs (Kamçı et al. 2022; Moses 2014; Rajesh et al. 2018; Saif et al. 2016; Wazir et al. 2022; Yaprak 2019). Absorption band was determined at 829 cm^{-1} caused by vibrations of Cu. The characteristic FTIR peaks were found at 3,260 (O–H stretching), 1,595 (C=O stretching), 1,561 (C=N stretching), 1,475 (C=C stretching), 1,360 (C–C stretching), 1,122 (C–O stretching), 815 (C–H stretching), and 640 (C–H stretching) cm^{-1}, respectively.

The changes seen between the FTIR spectra of dried plant extracts and the FTIR spectra of synthesized NPs are

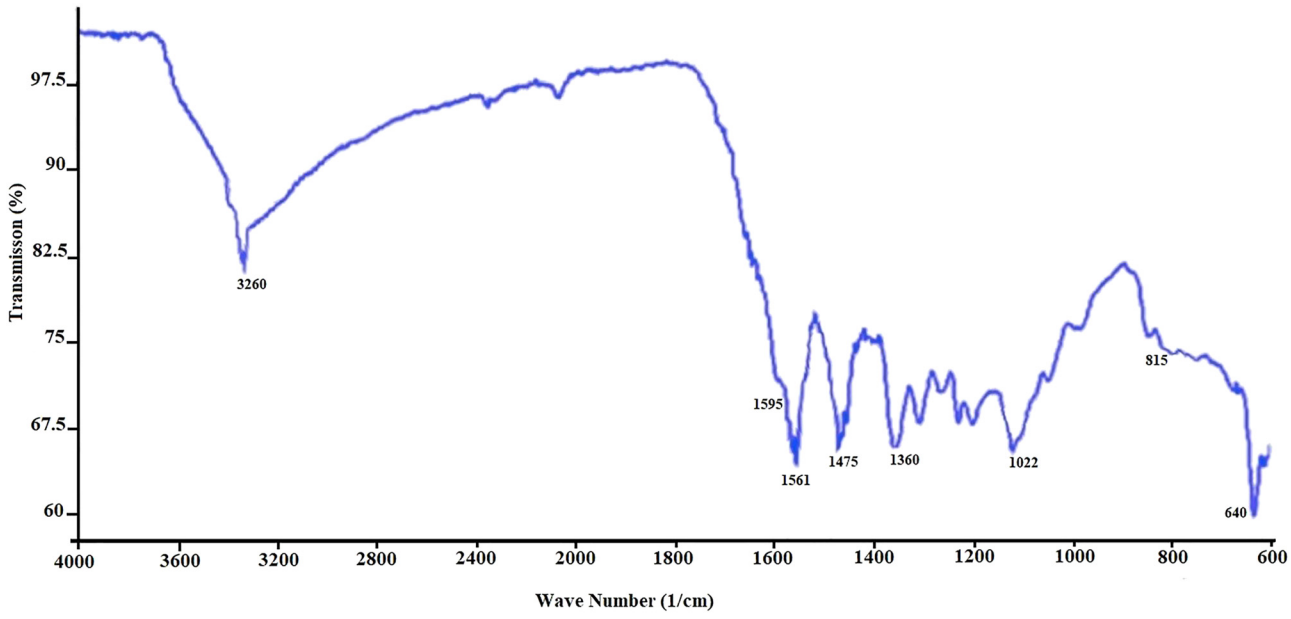

Figure 3: FTIR spectrum of *Moringa* extract-based CuNPs.

due to the participation of various functional groups in the ion exchange reaction. These functional groups act as biomolecules that cap, stabilize, and reduce NPs. As a result, the existence of different functional groups in the plant extract used for the synthesis of NPs was revealed. The peaks formed may be interpreted as the vibration of absorption bands observed in wavelengths (Ghareib et al. 2019; Kamçı et al. 2022; Rajesh et al. 2018; Saif et al. 2016; Sapsford et al. 2011; Wazir et al. 2022). The FTIR result obtained was compatible with the results stated in the literature. The results obtained are in agreement with scientific studies revealing the presence of biomolecules such as proteins and phytochemical components in plant extracts that play an important role in the reduction as well as coating agents on the surface of CuNPs. These surface-covering substances originating from plants form a layer that stabilizes the environment by preventing NPs from aggregating, and it is stated in some studies that they physically cover NPs (Asghar and Asghar 2020; Rajagopal et al. 2021). The results obtained in this study indicate that there was no chemical bond between the *Moringa* extract-based CuNPs and substrate materials and that the interaction between them was a physical bond. Based on these results, it is clear that metabolites and plant phytochemicals play an important role in the reduction of CuNPs.

The XRD analysis of CuNPs in the organic biomatrix was confirmed via XRD analysis as shown in Figure 4. The X-ray powder diffraction pattern of CuNPs showed intense peaks corresponding to (111), (200), (220), (311), and (222) Bragg's reflection based on the crystallinity of CuNPs. The XRD pattern of the CuNPs in Figure 4 shows that all the detected diffractions can be indexed to the crystal structure of zero valence copper (JCPDS card no. 4–836). The structural refinement yielded a cell parameter a:3.612 Å, which is near to the reported standard of a:3.615 Å. XRD peaks are compatible with metallic CuNPs. In addition, it is clear that the green synthesized nanoparticles exist as pure CuNPs without any contamination (Eltarahony et al. 2018; El Zowalaty et al. 2013). The peaks occurring at 2θ = 17.3° and 25.5° were formed by the presence of organic compounds in *M. oleifera* leaves (Ahmad et al. 2022; Karabulut et al. 2023). It is observed that the nanoparticles obtained exhibited severe crystal reflections. All the diffraction peaks in the figure belong to pure face-centered cubic copper. The lack of any oxide or impurity peak indicates the purity of the sample obtained (Ahmad et al. 2021; Ali et al. 2023; Biçer and Şişman 2010; Eltarahony et al. 2018; El Zowalaty et al. 2013; Saranyaadevi et al. 2014). All peaks of CuNPs can be indexed to the crystallographic parameters of

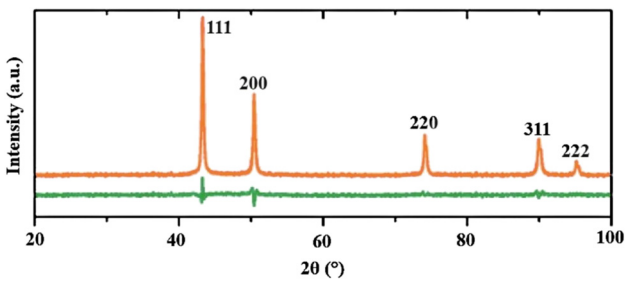

Figure 4: XRD pattern of *Moringa* extract-based CuNPs.

Cu in the monoclinic crystal system. The crystal size below 100 nm indicated that the nanocrystal structure of the biosynthesized CuNPs was at the nanoscale. Similar results were reported by other researchers in structure analysis of XRD for biosynthesized CuNPs (Ghidan et al. 2016; Rajagopal et al. 2021; Sharma et al. 2018).

The SEM analyzes were performed to detect the particle distribution and size of the pure *Moringa* extract and *Moringa* extract-based CuNPs. Figure 5a–d shows the SEM images of the pure *Moringa* extract and *Moringa* extract-based CuNPs taken at different magnifications, respectively. When the SEM micrograph images of pure *Moringa* particles are examined in Figure 5a and b, it is clearly seen that they have irregular shapes and are not uniform. In the same images, it is also seen that the surfaces are wrinkled and the particles are clumped. SEM images given in Figure 5c and d show that the CuNPs are quasi-spherical and most of them have diameters between 100 and 200 nm. It also reveals the presence of some larger particles of Cu NPs, which will cause the smaller particles to aggregate or overlap (Figure 5d). Available reports on NP synthesis using plant extracts also demonstrate the size diversity of NPs. Some studies have reported the presence of NPs with sizes ranging from 100 to 800 nm (Abbasifar et al. 2020). It is observed that even though there were nanoparticle agglomerations in some regions, they generally showed a homogenous distribution in the matrix. Moreover, it is observed that they consisted of spherical and nearly spherical-shaped nanoparticles and that their sizes were very small. It is observed that the CuNPs in the organic biomatrix were in the range of about

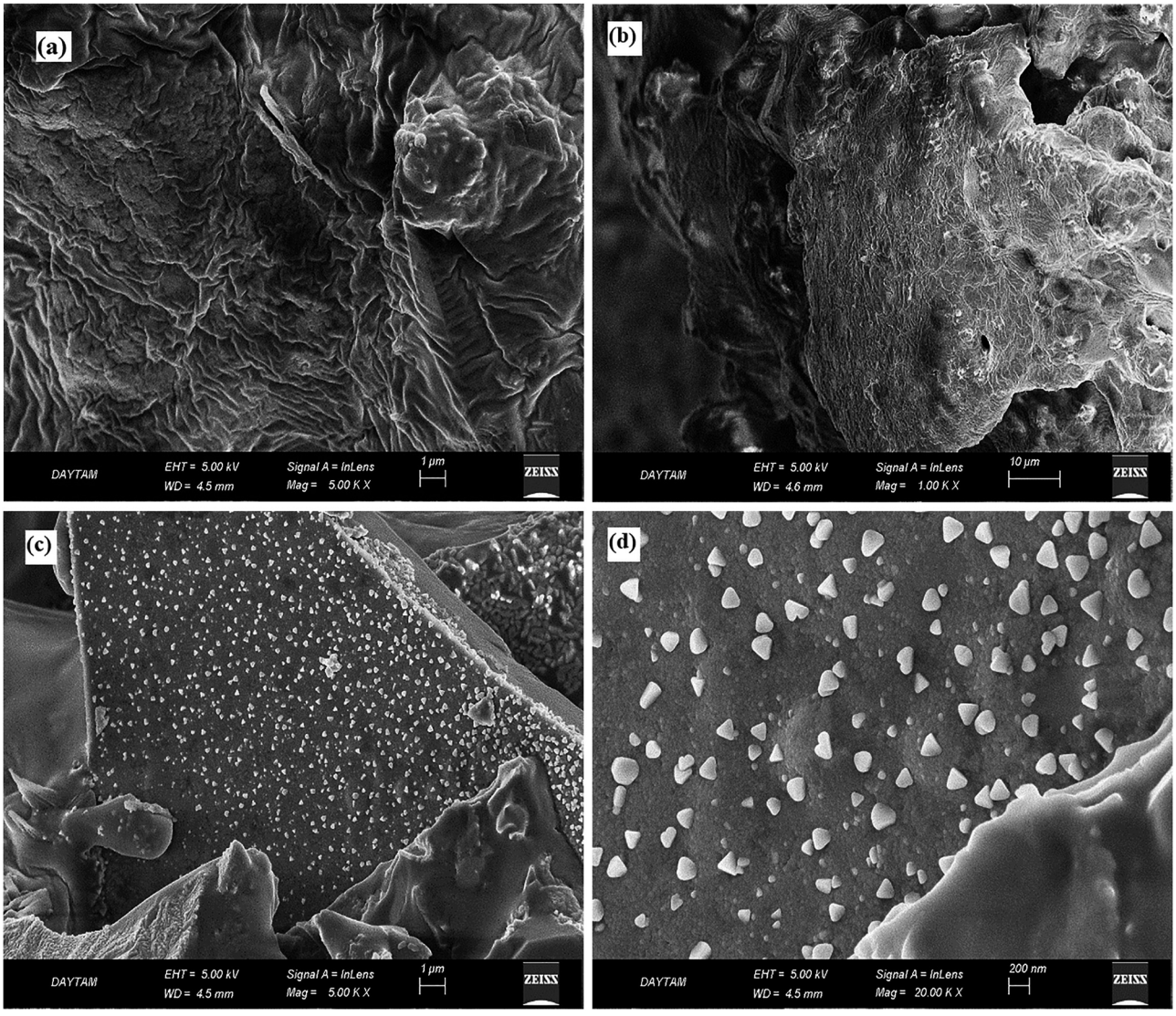

Figure 5: SEM images of (a) and (b) the pure *Moringa* extract; (c) and (d) *Moringa* extract-based CuNPs.

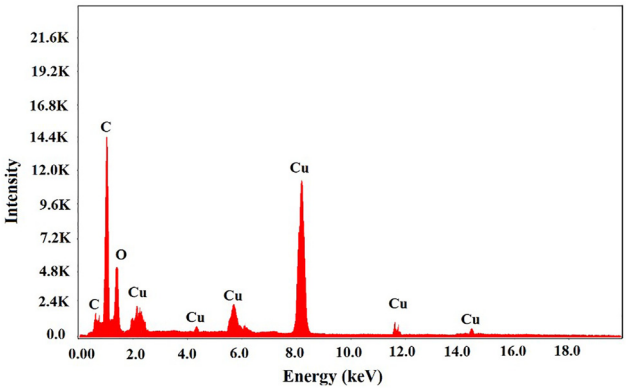

Figure 6: EDS spectrum analyses of the CuNPs.

10–150 nm. During synthesis, copper particles tend to agglomerate due to the high binding affinity of copper. Apart from this, agglomeration may also be caused by the high surface area of copper nano-sized particles (Biçer and Şişman 2010; El Zowalaty et al. 2013; Usman et al. 2012). According to this result, it is observed that the ones obtained from the FTIR analysis were compatible.

EDS analysis results obtained from SEM images are shown in Figure 6. The presence of Cu atoms is attributed to the formation of CuNPs, while the presence of C atoms is believed to be due to the plant extract, and the presence of O atoms is thought to result from the oxidation of Cu ions. The presence of some peaks such as C and O also indicates the presence of some biomolecules on the surface of metallic CuNPs (Rajesh et al. 2018). The EDS spectrum of green synthesized NPs shows a higher intense peak, which indicates that Cu element with the atomic percentage of 82.2 % as the main peak, which is in agreement with the key identification of Cu NPs. Similar observations have been reported in studies of the green synthesized CuNPs (Punniyakotti et al. 2020; Soofivand and Salavati-Niasari 2013).

3.2 Characterization of the CuNPs-coated Ti6Al4V

In broad terms, the combination of increased surface area and reduced microporosity resulting from the surface property of NPs plays an important role in the development and advancement of titanium-based implants, which are extensively used in the biomedical field for biomedical applications. SEM images of the CuNPs single-coated Ti6Al4V specimen and CuNPs double-coated Ti6Al4V specimen are given in Figure 7a and b, respectively. As understood from the SEM images of surface-modified Ti6Al4V with single and double-coating, it is observed that after coating, the CuNPs transformed to needle form from spherical form. In the single-coating images, it is observed that the CuNPs concentrated regionally, and in the double-coating images, it is observed that the needle-like construct exhibited a more compact and homogeneous distribution. And it is considered that the cracks shown in the SEM image were thermal cracks due to the postcoating drying of the samples in a drying oven. This status may be eliminated with a more controlled drying (Eltarahony et al. 2018). Shrinkage in the coating layer during the drying of the coating causes crack formation. In addition, the difference between the thermal expansion coefficients of the coated metal surface and the coating material, the heating and cooling cycles in the drying process also cause crack formation (Albayrak et al. 2019). The results obtained showed that controlling crack formation may be possible by optimizing the drying process (such as drying temperature, holding time, drying and cooling rate). Cracks in the coating can be perceived as a defect in terms of crack propagation during coating operation. However, cracks formed can be beneficial by relieving stresses during solidification and preventing spills (Çömez 2020).

EDS analysis results of the CuNPs single-coated Ti6Al4V and CuNPs double-coated Ti6Al4V specimens obtained from

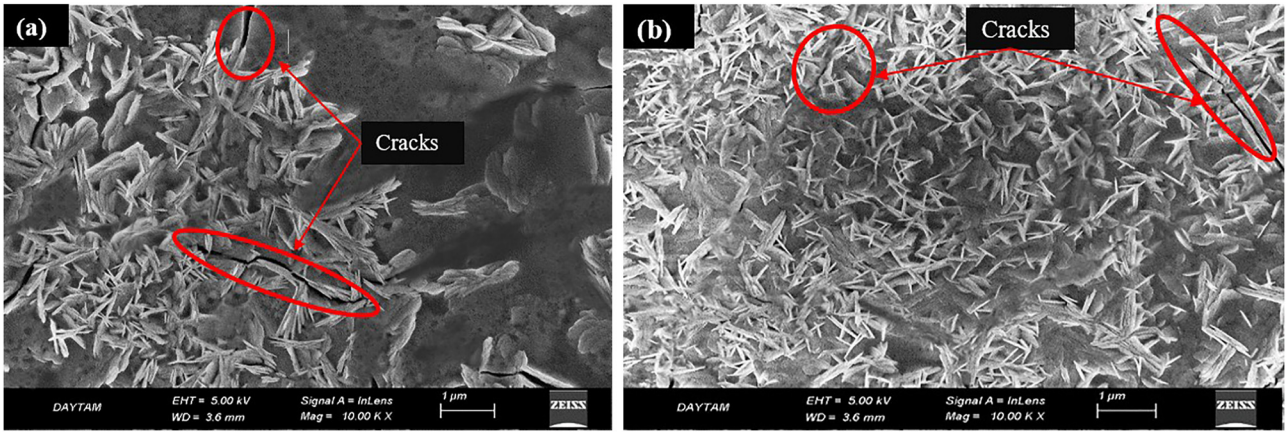

Figure 7: SEM images of the CuNPs-coated Ti6Al4V surfaces: (a) single-coated and (b) double-coated.

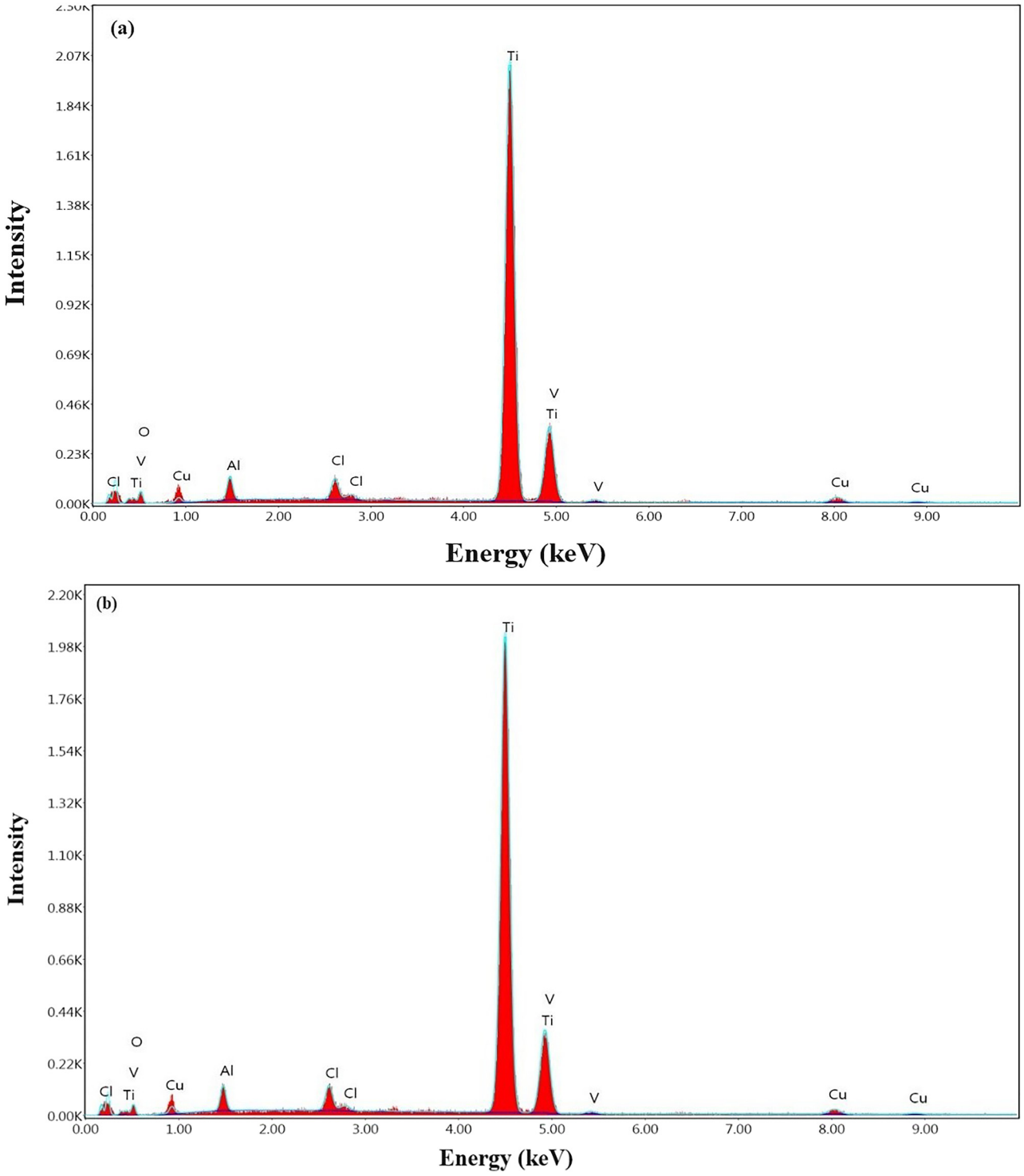

Figure 8: EDS analyses of the CuNPs-coated Ti6Al4V surfaces: (a) single-coated and (b) double-coated.

the SEM images are shown in Figure 8a and b, respectively. The presence of Cu is definitely due to the formation of CuNPs, while the presence of O atoms is thought to result from both the plant extract and CuNPs oxidation, while the presence of Cl atoms is thought to be due to the plant extract. Ti, Al, and trace amounts of V atoms in the coated surface are from the elemental signatures of Ti6Al4V substrate material. In the study conducted by Biçer and Şişman on the characterization of CuNPs, similar approaches have been mentioned (Biçer and Şişman 2010).

The average surface roughness values (Ra) of the noncoated, single-coated, and double-coated Ti6Al4V surfaces are given in Figure 9 for comparison. Noncoated, single-coated, and double-coated Ti6Al4V surfaces had Ra values of approximately 0.702, 0.533 µm, and 0.639 µm, respectively. When the surface roughness measurement results were evaluated, it was determined that the surface roughness value of single- and double-coated surfaces was smaller than the noncoated surface. This may have been caused by the measurement at the micron level and the nano-size of the coating particles. It was determined that the surface roughness value was higher on the double-coated surface. A high surface roughness within certain ranges is a demanded feature for the surfaces of metallic-based biomedical parts. With the surface roughness increasing up to a certain value, the spreading, adhesion, and growth of the cells are provided well and the adhesion of bacteria is prevented (Afewerki et al. 2020). In the literature, the surface roughness value for biomaterials varies between 0.5 and 1 µm (Liguori et al. 2022). In the light of these explanations, the surfaces obtained with various metallic nano-coatings have suitable surface roughness values and are promising for use in biomedical fields. According to some studies in the literature, it affects many specific properties of the coating such as surface roughness properties, and interaction with hydrophobic, bacterial, and abrasives (Jothi et al. 2022; Karabulut et al. 2023). All these aforementioned properties are improved by varying surface roughness. Similar approaches and the roughness values obtained according to this study are significant in biomaterial applications.

3.3 Electrochemical corrosion test results

Titanium alloys are known as materials having very high corrosion resistance. Titanium is very close to aluminum with its galvanic character value of 1.63 V. For this reason, it cannot be said that titanium has a superior pedigree structure. On the other hand, it is known that titanium exhibits superior corrosion resistance in different usage environments. The main reason for this is the stable and protective TiO_2 layer forming on the surface of titanium (Leyens and Peters 2003). It is very important to search for the effect of coating treatment on corrosion properties besides its effects on other properties. In line with this purpose, it was decided to perform a corrosion test. The result of the Open Circuit Potential (OCP) test and Tafel curve of the noncoated, single-coated, and double-coated Ti6Al4V substrates is shown in Figure 10a and b, respectively, of Ti6Al4V alloy is shown. The main purpose of OCP measurement tests is to measure the potential of the materials against corrosion under the relevant test conditions and to determine the potential of forming a stable surface film. When the (OCP)-time graph in Figure 10a is examined, it is observed that the coating forms a protective film on the surfaces. While the OCP value was −0.35 (V) in noncoated control material, it is observed that it moves toward −0.22 (V) as the result of single-coating with CuNPs. The standard deviation determined for OSP tests is between 5 and 10 mV. It was determined that the surface film layer forming as the result of a single coating preserves itself with an increase of 37.14 %. It is observed that the OCP value increases up to −0.18 (V) by the increase of the coating thickness. It was determined that the surface film layer forming as the result of double-coating with CuNPs protects by an 18 % increase compared to single-coated samples, and by a 49 % increase compared to noncoated control samples. The results are in agreement with similar studies in the literature (Abdulsada and Hammood 2021; Alves et al. 2009; Gu et al. 2018; Gurrappa 2003; S. Zhang et al. 2021).

Another test performed for observing the changes in the corrosion resistance of Ti6Al4V alloy is the potentiodynamic

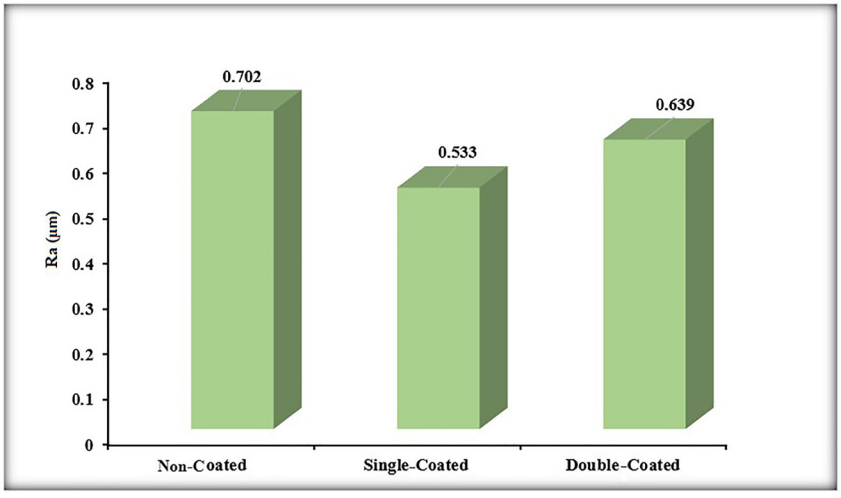

Figure 9: Comparison of surface roughness values of the noncoated, single-coated, and double-coated Ti6Al4V surfaces.

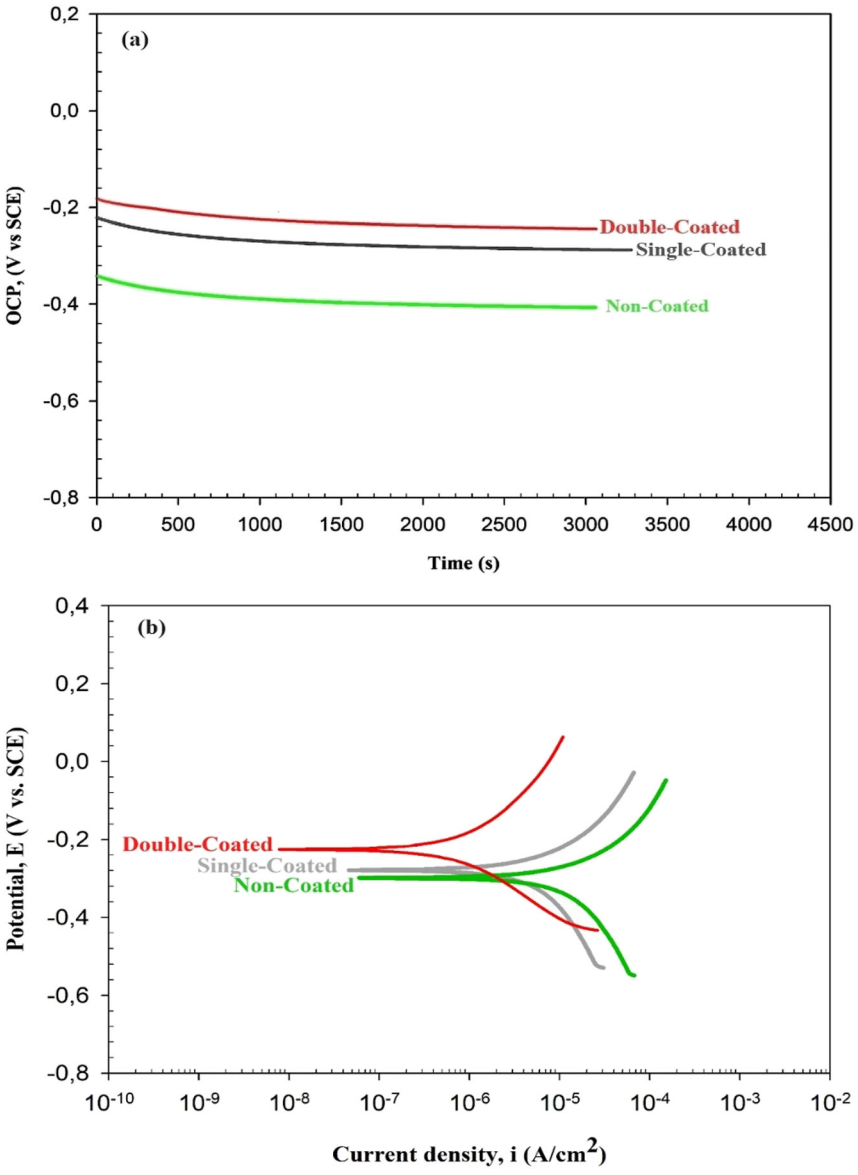

Figure 10: Corrosion test results (a) OCP and (b) Tafel curve of the noncoated, single-coated, and double-coated Ti6Al4V substrates.

polarization test. In Figure 10b, I_{corr} and E_{corr} values were determined via the software of the test device using the Tafel method. When the Tafel curve graph given in Figure 10b is examined, it is observed that curves with different coating amounts are similar to each other. In the field of corrosion research, it is expressed as low corrosion current and high corrosion potential, low corrosion rate and high corrosion resistance (He et al. 2019; Matik 2019). In the results of the Tafel curve obtained, it is clearly observed that the potential moves toward the cathodic region by the increase of CuNPs-coated surface. It is understood that the passivation tendency of the corrosion surface decreases by the movement of the potential of the Tafel curve toward the cathodic region as the result of coating. But when the values obtained are examined, it is observed that corrosion resistance is lower in noncoated Ti6Al4V control samples. According to the Tafel curves, by the increase of coating, the highest corrosion rate was obtained in noncoated Ti6Al4V alloys, and the lowest corrosion rate was obtained in the double-coated surface. The results obtained are consistent with similar studies in the literature (Cui et al. 2023; He et al. 2019; Matik 2019).

3.4 Antibacterial test results

The regular use of CuNPs in the organic biomatrix for innovative biomedical applications has been noted in many studies (Liu et al. 2020; Van Hengel et al. 2020). Within the scope of bioactivity tests, antibacterial and cytotoxicity tests of noncoated Ti6Al4V alloy as material control and CuNPs

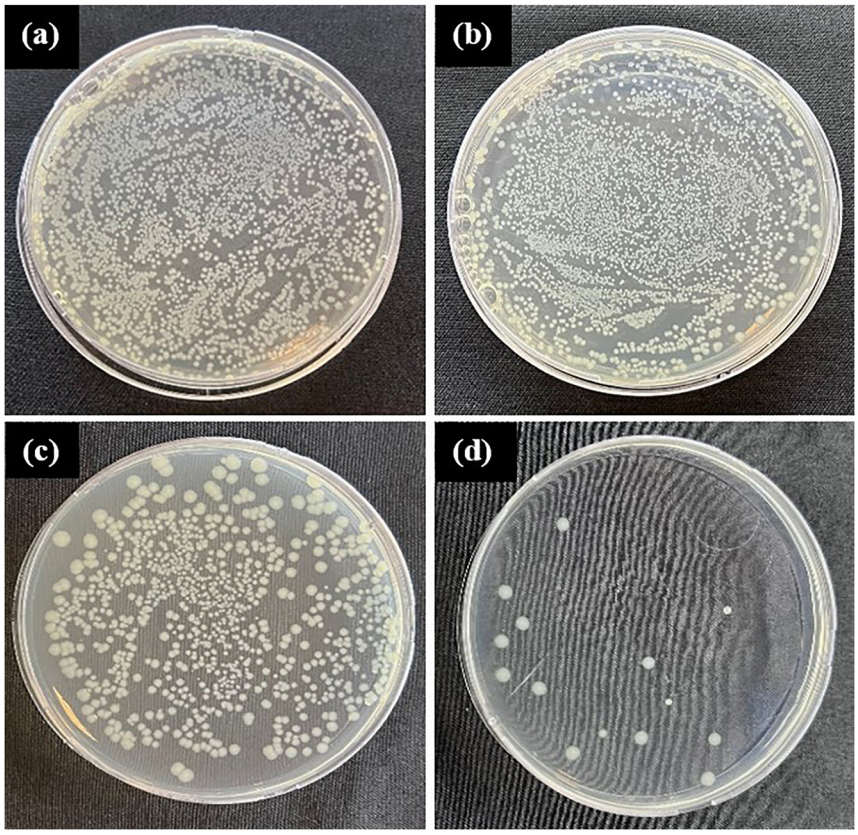

Figure 11: Antibacterial test results of 24 h: (a) *Escherichia coli* control, (b) noncoated Ti6Al4V alloy control, (c) CuNPs single-coated Ti6Al4V alloy, and (d) CuNPs double-coated Ti6Al4V alloy.

single-coated Ti6Al4V alloy and CuNPs double-coated Ti6Al4V alloy samples were performed. In the antibacterial test, only bacteria strains (*S. aureus* and *E. coli*) were tested as antibacterial test control, noncoated Ti6Al4V alloy as material control, and CuNPs single-coated Ti6Al4V alloy and CuNPs double-coated samples of Ti6Al4V alloy were tested. Antibacterial test results of control, sample control, single-coating, and double-coating samples at 24 h are given in Figure 11 as *E. coli* and in Figure 12 as *S. aureus*.

The density of colony numbers and antibacterial properties are inversely proportional. When the results of the samples in Figures 11 and 12 were evaluated, it was determined that the antibacterial activity varied according to the CuNPs coating, which is the coating material. Accordingly, it is seen that the CuNPs coating, which is common in the samples, shows antibacterial activity. While the most effective antibacterial activity on *E. coli* was seen in CuNPs double-coating, less antibacterial activity was observed in CuNPs single coating compared to CuNPs double-coating. As seen from the results, the antibacterial properties of the samples increase as the coating of the samples increases. Also, no significant difference was observed between the strains. However, it was clearly observed that the samples showed antibacterial activity on *E. coli* and *S. aureus* strains. In Figure 13, the kill % results for *E. coli* and *S. aureus* on the test samples is given. According to the study of Fuentes et al. (Fuentes et al. 2021), it was observed that CuNPs-coated TiO_2 nanocomposites had an effective antibacterial activity on *S. aureus*. According to the study of Devi et al. (Devi et al. 2019), biodegradable poly (propylene) carbonate using CuNPs-coated *Tamarindus indica* filler exhibited effective antibacterial behavior against *E. coli* and *P. aeruginosa*, *B. licheniformis*, and *S. aureus*. With these studies we mentioned, it is seen that the coating of the biomaterial with CuNPs increases the antibacterial activity.

3.5 Cytotoxic tests results

As seen in Figure 14, Ti6Al4V samples single- and double-coated did not adversely affect their biocompatibility compared to the noncoated control sample. It was determined that the cytotoxic effect increased with increasing coating layer. Cell viability increased in direct proportion with the increasing number of days on all Ti6Al4V alloy surfaces with single-coated, double-coated, and noncoated. This shows that our material may have

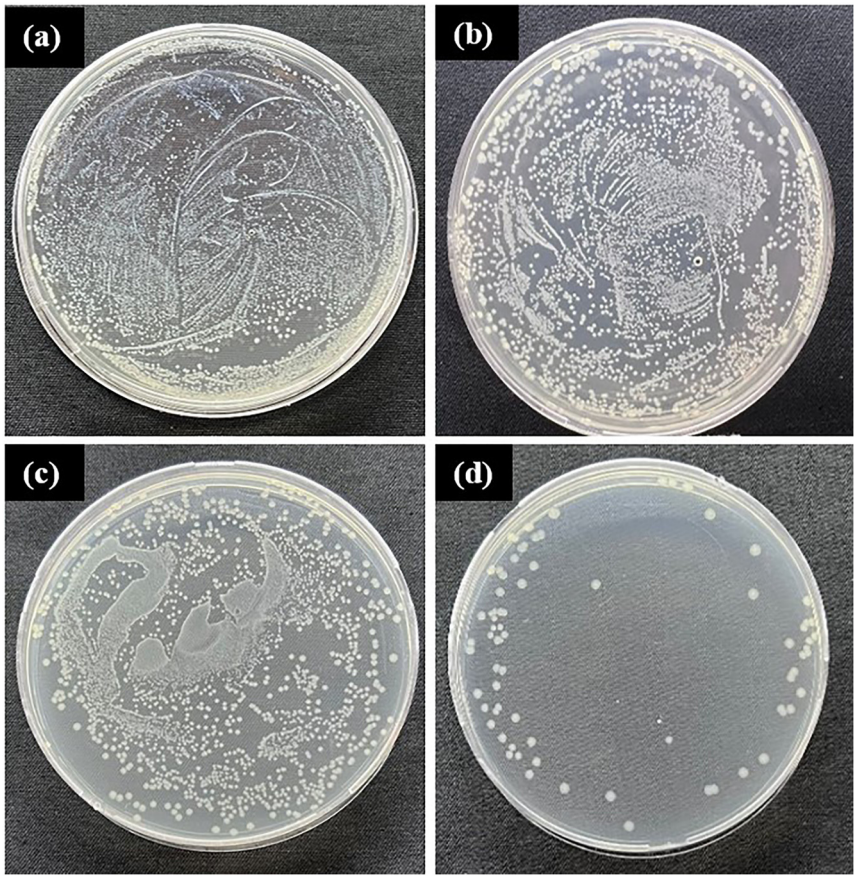

Figure 12: Antibacterial test results of 24 h: (a) *Staphylococcus aureus* control, (b) noncoated Ti6Al4V alloy control, (c) CuNPs single-coated Ti6Al4V alloy, and (d) CuNPs double-coated Ti6Al4V alloy.

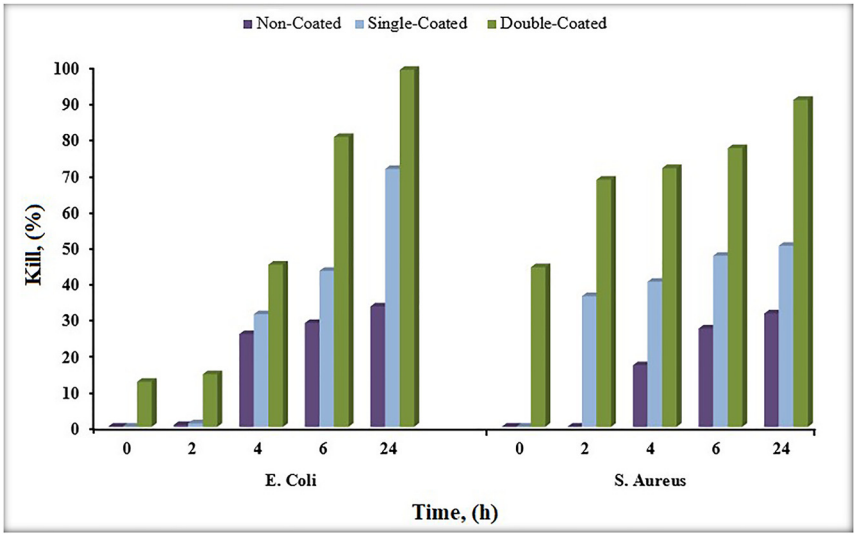

Figure 13: Kill % results for *Escherichia coli* and *Staphylococcus aureus* on the test samples.

tolerable biocompatibility in the body. According to the study of Korniienko et al. (Korniienko et al. 2020), it was determined that the ZrNb alloy with PEO oxide coatings containing CuNPs in the organic biomatrix was more biocompatible than the noncoated alloy after 7 days of cell incubation. According to the study of Thukkaram et al. (Thukkaram et al. 2021), when the effect of Ti discs coated with amorphous hydrocarbon (a-C:H) thin layer containing CuNPs on MC3T3 cells was examined after 7 days of incubation, the material was found to be biocompatible. With these studies we mentioned, it is seen that coating the biomaterial with CuNPs increases biocompatibility.

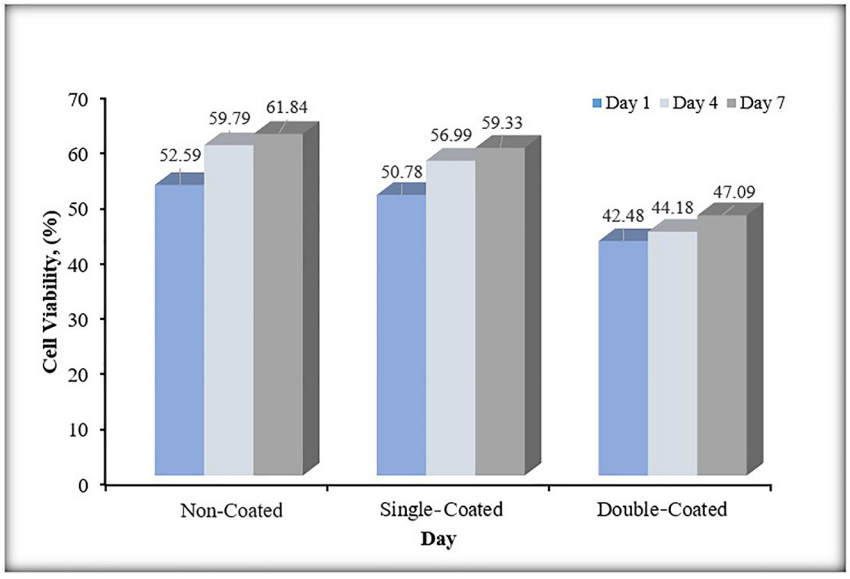

Figure 14: MTT test results.

4 Conclusions

The main aim of this study was to focus anticorrosive, antibacterial, and biocompatibility features of Ti6Al4V alloy coated with the green synthesized CuNPs. The surface-modified Ti6Al4V alloys with single and double organic nanostructures coating was characterized by the multi-faceted investigations. The results obtained from the present study are given below:

- According to the UV–Vis results, the width of the bands of CuNPs is an indication that the particles exhibit a polydisperse distribution.
- In the FTIR spectra of CuNPs, vibrations varying in the range of 600–1,600 cm^{-1} were observed belonging to the Cu vibrations confirming the formation of CuNPs.
- In the XRD analysis of CuNPs, the lack of any oxide or impurity peak indicated the purity of the sample obtained.
- SEM results of single- and double-coated CuNPs showed that Cu nanoparticles transformed from spherical forms to needle forms following coating. The sizes of Cu nanoparticles were measured as 10–150 nm.
- In the EDS analysis, the presence of Cu is due to the formation of CuNPs, while the presence of O atoms is thought to be result of both the plant extract and CuNPs oxidation, while the presence of Cl atoms is thought to be due to the plant extract. The results of the SEM-EDS, FTIR, and XRD analyses in this investigation were found to be consistent with earlier literature studies.
- It was determined that the surface roughness value of the coated Ti6Al4V substrates with single- and double-coating was lower than the noncoated surface.
- The OCP biocorrosion test results showed that the coating created a protective film on the surfaces. The thickness of the coating was correlated with an improvement in corrosion resistance.
- According to Tafel curve results, it was clearly observed that the potential moves toward the cathodic region by an increase of CuNPs coating which in turn resulting a proportional increase in corrosion resistance.
- According to the antibacterial test results, it was observed that the antibacterial activity was similar in both strains (*S. aureus* and *E. coli*) according to the coating material CuNPs coating. The activity increased with the increase in the thickness of the coating.
- Anticorrosion coatings with nanoscale morphology to implant surfaces are one of the efficient, flexible, cost-effective, and straightforward strategies. This study focused on the corrosion properties of surface-modified Ti6Al4V with green synthesized CuNPs. The results illustrated the importance of surface modification in attaining favorable corrosion resistance. Small particle size, uniform distribution, light particle agglomeration, and smooth surfaces provided better corrosion protection.
- Biocompatibility results showed that the samples coated with single and double CuNPs maintained their viability, although less than the noncoated control. However, as the coating increases, the cytotoxic effect also increases. Additionally, it was shown that cell viability increased with time in all single-coated, double-coated, and non-coated materials in direct proportion. The material in this case shows that it may have a tolerable biocompatibility in the body.

Acknowledgments: We are grateful to Assoc. Prof. Dr. Selcan KARAKUŞ, Istanbul University-Cerrahpasa, for providing Moringa oleifera leaf.

Research ethics: Not applicable.

Informed consent: Not applicable.

Author contributions: Conceptualization, Ş.A., S.E., and N.B.Ü.; methodology, Ş.A., N.B.Ü., and S.C.A.; validation, Ş.A. and S.E.; formal analysis, Ş.A., S.E., S.C.A., and N.E.; investigation, Ş.A., S.E., and N.E.; writing—original draft preparation, Ş.A., N.B.Ü., and S.C.A.; writing—review and editing, Ş.A., S.E., and N.B.Ü.; supervision, Ş.A.; project administration, Ş.A. and N.B.Ü. All authors have read and agreed to the published version of the manuscript.

Use of Large Language Models, AI and Machine Learning Tools: None declared.

Conflict of interest: The authors state no conflict of interest.

Research funding: This study was funded by Scientific Research Projects Coordination Unit of Istanbul University-Cerrahpaşa. Project number: FYL-2021-35633.

Data availability: Not applicable.

References

Abbasifar, A., Shahrabadi, F., and ValizadehKaji, B. (2020). Effects of green synthesized zinc and copper nano-fertilizers on the morphological and biochemical attributes of basil plant. *J. Plant Nutr.* 43: 1104–1118.

Abdulsada, F.W. and Hammood, A.S. (2021). Characterization of corrosion and antibacterial resistance of hydroxyapatite/silver nano particles powder on 2507 duplex stainless steel. *Mater. Today Proc.* 42: 2301–2307.

Acar Derman, S., Akdeste, Z., Canim Ates, S., Mansuroglu (Mansour Karaman), B., Kizilbey, K., Bagirova, B., and Allahverdiyev, A. (2017). The study of synthetic peptide loaded PLGA nanoparticles vcytotoxicity in vitro. *Fresenius Environ. Bull.* 26: 8.

Afewerki, S., Bassous, N., Harb, S., Palo-Nieto, C., Ruiz-Esparza, G.U., Marciano, F.R., Webster, T.J., Furtado, A.S.A., and Lobo, A.O. (2020). Advances in dual functional antimicrobial and osteoinductive biomaterials for orthopaedic applications. *Nanomed. Nanotechnol. Biol. Med.* 24: 102143.

Ahmad, A., Khan, M., Khan, S., Luque, R., Abualnaja, K.M., Alduaij, O.K., and Yousef, T.A. (2022). Bio-construction of CuO nanoparticles using Texas sage plant extract for catalytical degradation of methylene blue via photocatalysis. *J. Mol. Struct.* 1256: 132522.

Ahmad, S., Ali, S., Ullah, I., Zobaer, M.S., Albakri, A., and Muhammad, T. (2021). Synthesis and characterization of manganese ferrite from low grade manganese ore through solid state reaction route. *Sci. Rep.* 11: 16190.

Albayrak, Ö., İpekoğlu, M., and Altıntaş, S. (2019). Üretim parametrelerinin hidroksiapatit tozlarının özellikleri ve kaplama kalitesi üzerindeki etkilerinin incelenmesi. *Çukurova Üniversitesi Mühendislik-Mimarlık Fakültesi Dergisi* 34: 243–256.

Ali, S., Ahmad, S., Ali, S.A., Khalid, L., and Ullah, I. (2023). Synthesis and characterization of lithium manganese oxide (LiMn2O4) from manganese ore via solid state reaction route. *Pakistan J. Sci. Ind. Res. Ser. A: Phys.Sci.* 66: 221–226.

Alias, R., Mahmoodian, R., and Abd Shukor, M.H. (2019). Development and characterization of a multilayer silver/silver-tantalum oxide thin film coating on stainless steel for biomedical applications. *Int. J. Adhes. Adhes.* 92: 89–98.

Alves, V.A., Reis, R.Q., Santos, I.C.B., Souza, D.G., de, F., Gonçalves, T., Pereira-da-Silva, M.A., Rossi, A., and da Silva, L.A. (2009). In situ impedance spectroscopy study of the electrochemical corrosion of Ti and Ti–6Al–4V in simulated body fluid at 25°C and 37°C. *Corros. Sci.* 51: 2473–2482.

Asghar, M.A. and Asghar, M.A. (2020). Green synthesized and characterized copper nanoparticles using various new plants extracts aggravate microbial cell membrane damage after interaction with lipopolysaccharide. *Int. J. Biol. Macromol.* 160: 1168–1176.

Asri, R.I.M., Harun, W.S.W., Samykano, M., Lah, N.A.C., Ghani, S.A.C., Tarlochan, F., and Raza, M.R. (2017). Corrosion and surface modification on biocompatible metals: a review. *Mater. Sci. Eng., C* 77: 1261–1274.

Bai, X., Li, J., and Zhu, L. (2019). Structure and properties of TiSiN/Cu multilayer coatings deposited on Ti6Al4V prepared by arc ion plating. *Surf. Coat. Technol.* 372: 16–25.

Begum, N.A., Mondal, S., Basu, S., Laskar, R.A., and Mandal, D. (2009). Biogenic synthesis of Au and Ag nanoparticles using aqueous solutions of Black Tea leaf extracts. *Colloids Surf., B: Biointerfaces* 71: 113–118.

Benakashani, F., Allafchian, A.R., and Jalali, S.A.H. (2016). Biosynthesis of silver nanoparticles using Capparis spinosa L. leaf extract and their antibacterial activity. *Karbala Int. J. Mod. Sci.* 2: 251–258.

Biçer, M. and Şişman, İ. (2010). Controlled synthesis of copper nano/microstructures using ascorbic acid in aqueous CTAB solution. *Powder Technol.* 198: 279–284.

Bocchetta, P., Chen, L.Y., Tardelli, J.D.C., Reis, A.dos, Almeraya-Calderón, F., and Leo, P. (2021). Passive layers and corrosion resistance of biomedical Ti-6Al-4V and β-Ti alloys. *Coatings* 11: 487.

Cai, Y., Luo, X., Maclean, M., Qin, Y., Duxbury, M., and Ding, F. (2019). A single-step fabrication approach for development of antimicrobial surfaces. *J. Mater. Process. Technol.* 271: 249–260.

Calabrese, C., La Parola, V., Testa, M.L., and Liotta, L.F. (2022). Antifouling and antimicrobial activity of Ag, Cu and Fe nanoparticles supported on silica and titania. *Inorg. Chim. Acta* 529: 120636.

Chen, L., Wang, D., Qiu, J., Zhang, X., Liu, X., Qiao, Y., and Liu, X. (2021). Synergistic effects of immunoregulation and osteoinduction of ds-block elements on titanium surface. *Bioact. Mater.* 6: 191–207.

Chen, Q. and Thouas, G.A. (2015). Metallic implant biomaterials. *Mater. Sci. Eng.: R: Rep.* 87: 1–57.

Cheng, Y.H., Browne, T., Heckerman, B., and Meletis, E.I. (2010). Mechanical and tribological properties of nanocomposite TiSiN coatings. *Surf. Coat. Technol.* 204: 2123–2129.

Chou, W.-L., Yu, D.-G., and Yang, M.-C. (2005). The preparation and characterization of silver-loading cellulose acetate hollow fiber membrane for water treatment. *Polym. Adv. Technol.* 16: 600–607.

Çömez, N. (2020). WC-Ni sert dolgu alaşımının kuru ve NaCl çözelti ortamlarındaki aşınma performansı. *Dicle Üniversitesi Mühendislik Fakültesi Mühendislik Dergisi* 11: 553–562.

Cui, Y.-W., Chen, L.-Y., Chu, Y.-H., Zhang, L., Li, R., Lu, S., Wang, L., and Zhang, L.-C. (2023). Metastable pitting corrosion behavior and characteristics of passive film of laser powder bed fusion produced Ti–6Al–4V in NaCl solutions with different concentrations. *Corros. Sci.* 215: 111017.

Devi, M.I., Nallamuthu, N., Rajini, N., Kumar, T.S.M., Siengchin, S., Rajulu, A.V., and Ayrilmis, N. (2019). Biodegradable poly (propylene)

carbonate using in-situ generated CuNPs coated Tamarindus indica filler for biomedical applications. *Mater. Today Commun.* 19: 106–113.

Duman, F., Ocsoy, I., and Kup, F.O. (2016). Chamomile flower extract-directed CuO nanoparticle formation for its antioxidant and DNA cleavage properties. *Mater. Sci. Eng. C* 60: 333–338.

El hadad, A.A., García-Galván, F.R., Mezour, M.A., Hickman, G.J., Soliman, I.E., Jiménez-Morales, A., Barranco, V., Galván, J.C., and Perry, C.C. (2020). Organic-inorganic hybrid coatings containing phosphorus precursors prepared by sol–gel on Ti6Al4V alloy: electrochemical and in-vitro biocompatibility evaluation. *Prog. Org. Coat.* 148: 105834.

El Zowalaty, M., Ibrahim, N.A., Salama, M., Shameli, K., Usman, M., and Zainuddin, N. (2013). Synthesis, characterization, and antimicrobial properties of copper nanoparticles. *Int. J. Nanomed.* 4467, https://doi.org/10.2147/ijn.s50837.

Eltarahony, M., Zaki, S., and Abd-El-Haleem, D. (2018). Concurrent synthesis of zero- and one-dimensional, spherical, rod-needle-and wire-shaped CuO nanoparticles by *Proteus mirabilis* 10B. *J. Nanomater.* 2018: e1849616.

Fernández-Arias, M., Boutinguiza, M., del Val, J., Riveiro, A., Rodríguez, D., Arias-González, F., Gil, J., and Pou, J. (2020). Fabrication and deposition of copper and copper oxide nanoparticles by laser ablation in open air. *Nanomaterials* 10: 300.

Freitas, T.S., Marques, T.M.F., Barros, L., da Silva, J.H., Cruz, R.P., Pereira, R.L.S., Silva, A.R.P., Santos, A.T.L., Ghosh, A., Agressott, E.V.H., et al. (2021). Synthesis of Cu-tint, characterization, and antibacterial properties evaluation. *Mater. Today Chem.* 21: 100539.

Fuentes, S., Tapia, A., and Pozo, P. (2021). Synthesis, characterization, and antibacterial activity evaluation of Cu@ TiO2 nanocomposites. *Mater. Lett.* 296: 129885.

Ghareib, M., Abdallah, W., Tahon, M.A., and Tallima, A. (2019). Biosynthesis of copper oxide nanoparticles using the preformed biomass of aspergillus fumigatus and their antibacterial and photocatalytic activities. *Dig. J. Nanomater. Biostruct.* 14: 291–303.

Ghidan, A.Y., Al-Antary, T.M., and Awwad, A.M. (2016). Green synthesis of copper oxide nanoparticles using Punica granatum peels extract: effect on green peach Aphid. *Environ. Nanotechnol. Monit. Manage.* 6: 95–98.

Gil, C., Villegas, M.A., and Navarro, J.M.F. (2006). TEM monitoring of silver nanoparticles formation on the surface of lead crystal glass. *Appl. Surf. Sci.* 253: 1882–1888.

Gnanavel, S., Ponnusamy, S., Mohan, L., and Muthamizhchelvan, C. (2018). In vitro corrosion behaviour of Ti–6Al–4V and 316L stainless steel alloys for biomedical implant applications. *J. Bio- Tribo-Corros.* 4: 1–8.

Gong, P., Li, H., He, X., Wang, K., Hu, J., Tan, W., Zhang, S., and Yang, X. (2007). Preparation and antibacterial activity of Fe3O4@Ag nanoparticles. *Nanotechnology* 18: 285604.

Gu, K.-X., Wang, K.-K., Zheng, J.-P., Chen, L.-B., and Wang, J.-J. (2018). Electrochemical behavior of Ti–6Al–4V alloy in Hank's solution subjected to deep cryogenic treatment. *Rare Met.* 42: 2037–2046.

Gurrappa, I. (2003). Characterization of titanium alloy Ti-6Al-4V for chemical, marine and industrial applications. *Mater. Charact.* 51: 131–139.

Hadidi, M., Bigham, A., Saebnoori, E., Hassanzadeh-Tabrizi, S.A., Rahmati, S., Alizadeh, Z.M., Nasirian, V., and Rafienia, M. (2017). Electrophoretic-deposited hydroxyapatite-copper nanocomposite as an antibacterial coating for biomedical applications. *Surf. Coat. Technol.* 321: 171–179.

He, X., Zhang, G., Wang, X., Hang, R., Huang, X., Qin, L., Tang, B., and Zhang, X. (2017). Biocompatibility, corrosion resistance and antibacterial activity of TiO2/CuO coating on titanium. *Ceram. Int.* 43: 16185–16195.

He, X., Song, R.G., and Kong, D.J. (2019). Microstructure and corrosion behaviour of laser-cladding Al-Ni-TiC-CeO2 composite coatings on S355 offshore steel. *J. Alloys Compd.* 770: 771–783.

Hidalgo-Robatto, B.M., López-Álvarez, M., Azevedo, A.S., Dorado, J., Serra, J., Azevedo, N.F., and González, P. (2018). Pulsed laser deposition of copper and zinc doped hydroxyapatite coatings for biomedical applications. *Surf. Coat. Technol.* 333: 168–177.

Huang, Q., Li, X., Elkhooly, T.A., Liu, X., Zhang, R., Wu, H., Feng, Q., and Liu, Y. (2018). The Cu-containing TiO2 coatings with modulatory effects on macrophage polarization and bactericidal capacity prepared by micro-arc oxidation on titanium substrates. *Colloids Surf., B: Biointerfaces* 170: 242–250.

Hussain, R.F., Nouri, A.M.E., and Oliver, R.T.D. (1993). A new approach for measurement of cytotoxicity using colorimetric assay. *J. Immunol. Methods* 160: 89–96.

Irzh, A., Perkas, N., and Gedanken, A. (2007). Microwave-assisted coating of PMMA beads by silver nanoparticles. *Langmuir* 23: 9891–9897.

Jin, G., Cao, H., Qiao, Y., Meng, F., Zhu, H., and Liu, X. (2014). Osteogenic activity and antibacterial effect of zinc ion implanted titanium. *Colloids Surf., B: Biointerfaces* 117: 158–165.

Jothi, K.J., Balachandran, S., and Palanivelu, K. (2022). Synergistic combination of Phyllanthus niruri/silver nanoparticles for anticorrosive application. *Mater. Chem. Phys.* 279: 125794.

Kamçı, H., Recep, T., and Çelebioğlu, H.U. (2022). Antibacterial activity of copper nanoparticles synthesized by using Peumus boldus leaf extract. *EJOSAT* 139–142, https://doi.org/10.31590/ejosat.1110891.

Karabulut, G., Üllen, N.B., Akyüz, E., and Karakuş, S. (2023). Surface modification of 316L stainless steel with multifunctional locust gum/polyethylene glycol-silver nanoparticles using different coating methods. *Prog. Org. Coat.* 174: 107291.

Korniienko, V., Oleshko, O., Husak, Y., Deineka, V., Holubnycha, V., Mishchenko, O., Kazek-Kęsik, A., Jakóbik-Kolon, A., Pshenychnyi, R., Leśniak-Zió\lkowska, K., et al. (2020). Formation of a bacteriostatic surface on ZrNb alloy via anodization in a solution containing Cu nanoparticles. *Materials* 13: 3913.

Köse, C., Kaçar, R., Zorba, A.P., Bağirova, M., Abamor, E.Ş., and Allahverdİyev, A.M. (2018). Interactions between fibroblast cells and laser beam welded AISI 2205 duplex stainless Steel. *Mater. Sci.* 24: 159–165.

Leyens, C. and Peters, M. (2003). *Titanium and titanium alloys: fundamentals and applications*. John Wiley & Sons, Weinheim, Germany, p. 544.

Li, T., Li, L., Qi, J., and Chen, F. (2020). Corrosion protection of Ti6Al4V by a composite coating with a plasma electrolytic oxidation layer and sol-gel layer filled with graphene oxide. *Prog. Org. Coat.* 144: 105632.

Liguori, A., Gino, M.E., Panzavolta, S., Torricelli, P., Maglio, M., Parrilli, A., Gualandi, C., Griffoni, C., Brodano, G.B., Fini, M., et al. (2022). Tantalum nanoparticles enhance the osteoinductivity of multiscale composites based on poly (lactide-co-glycolide) electrospun fibers embedded in a gelatin hydrogel. *Mater. Today Chem.* 24: 100804.

Liu, J., Liu, J., Attarilar, S., Wang, C., Tamaddon, M., Yang, C., Xie, K., Yao, J., Wang, L., Liu, C., et al. (2020). Nano-modified titanium implant materials: a way toward improved antibacterial properties. *Front. Bioeng. Biotechnol.* 8: 576969.

Lu, M., Zhang, Z., Zhang, J., Wang, X., Qin, G., and Zhang, E. (2021). Enhanced antibacterial activity of Ti-Cu alloy by selective acid etching. *Surf. Coat. Technol.* 421: 127478.

Mansuroğlu, B., Derman, S., Kızılbey, K., Ateş, S.C., and Akdeste, Z.M. (2020). Synthetic peptide vaccine for Foot-and-Mouth Disease: synthesis, characterization and immunogenicity. *Turk. J. Biochem.* 45: 859–868.

Matik, U. (2019). Corrosion resistance of electroless NiP/NiB duplex coating. In: *UDCS'19 Fourth International Iron and Steel Symposium, 4–6 April*. Karabuk University, Turkiye, pp. 10–12.

Mierzejewska, Ż.A., Hudák, R., and Sidun, J. (2019). Mechanical properties and microstructure of DMLS Ti6Al4V alloy dedicated to biomedical applications. *Materials* 12: 176.

Moses, V. (2014). Biological synthesis of copper nanoparticles and its impact - a review. *Int. J. Pharm. Sci. Res. Invention* 3: 06–28.

Nasrollahzadeh, M., Momeni, S.S., and Sajadi, S.M. (2017). Green synthesis of copper nanoparticles using Plantago asiatica leaf extract and their application for the cyanation of aldehydes using K4Fe (CN) 6. *J. Colloid Interface Sci.* 506: 471–477.

Navaladian, S., Viswanathan, B., Viswanath, R.P., and Varadarajan, T.K. (2007). Thermal decomposition as route for silver nanoparticles. *Nanoscale Res. Lett.* 2: 44.

Pan, J., Leygraf, C., Thierry, D., and Ektessabi, A.M. (1997). Corrosion resistance for biomaterial applications of TiO2 films deposited on titanium and stainless steel by ion-beam-assisted sputtering. *J. Biomed. Mater. Res.* 35: 309–318.

Perelshtein, I., Applerot, G., Perkas, N., Guibert, G., Mikhailov, S., and Gedanken, A. (2008). Sonochemical coating of silver nanoparticles on textile fabrics (nylon, polyester and cotton) and their antibacterial activity. *Nanotechnology* 19: 245705.

Prestat, M. and Thierry, D. (2021). Corrosion of titanium under simulated inflammation conditions: clinical context and in vitro investigations. *Acta Biomater*. 136: 72–87.

Punniyakotti, P., Panneerselvam, P., Perumal, D., Aruliah, R., and Angaiah, S. (2020). Anti-bacterial and anti-biofilm properties of green synthesized copper nanoparticles from Cardiospermum halicacabum leaf extract. *Bioprocess Biosyst. Eng*. 43: 1649–1657.

Quinn, J., McFadden, R., Chan, C.-W., and Carson, L. (2020). Titanium for orthopedic applications: an overview of surface modification to improve biocompatibility and prevent bacterial biofilm formation. *ISci* 23: 101745.

Rahimi, E., Offoiach, R., Baert, K., Terryn, H., Lekka, M., and Fedrizzi, L. (2021). Role of phosphate, calcium species and hydrogen peroxide on albumin protein adsorption on surface oxide of Ti6Al4V alloy. *Materialia* 15: 100988.

Rajagopal, G., Nivetha, A., Sundar, M., Panneerselvam, T., Murugesan, S., Parasuraman, P., Kumar, S., Ilango, S., and Kunjiappan, S. (2021). Mixed phytochemicals mediated synthesis of copper nanoparticles for anticancer and larvicidal applications. *Heliyon* 7, https://doi.org/10.1016/j.heliyon.2021.e07360.

Rajesh, K.M., Ajitha, B., Reddy, Y.A.K., Suneetha, Y., and Reddy, P.S. (2018). Assisted green synthesis of copper nanoparticles using Syzygium aromaticum bud extract: physical, optical and antimicrobial properties. *Optik* 154: 593–600.

Raza, M.R., Ahmad, F., Muhamad, N., Sulong, A.B., Omar, M.A., Akhtar, M.N., and Aslam, M. (2016). Effects of solid loading and cooling rate on the mechanical properties and corrosion behavior of powder injection molded 316 L stainless steel. *Powder Technol.* 289: 135–142.

Ren, L., Wong, H.M., Yan, C.H., Yeung, K.W.K., and Yang, K. (2015). Osteogenic ability of Cu-bearing stainless steel. *J. Biomed. Mater. Res. Part B: Appl. Biomater.* 103: 1433–1444.

Roguska, A., Kudelski, A., Pisarek, M., Opara, M., and Janik-Czachor, M. (2011). Surface-enhanced Raman scattering (SERS) activity of Ag, Au and Cu nanoclusters on TiO2-nanotubes/Ti substrate. *Appl. Surf. Sci.* 257: 8182–8189.

Saif, S., Tahir, A., Asim, T., and Chen, Y. (2016). Plant mediated green synthesis of CuO nanoparticles: comparison of toxicity of engineered and plant mediated CuO nanoparticles towards Daphnia magna. *Nanomaterials* 6: 205.

Sapsford, K.E., Tyner, K.M., Dair, B.J., Deschamps, J.R., and Medintz, I.L. (2011). Analyzing nanomaterial bioconjugates: a review of current and emerging purification and characterization techniques. *Anal. Chem.* 83: 4453–4488.

Saranyaadevi, K., Subha, V., Ravindran, R.S.E., and Renganathan, S. (2014). Synthesis and characterization of copper nanoparticle using Capparis zeylanica leaf extract. *Int. J. ChemTech Res.* 6: 4533–4541.

Shan, L., Zhang, Y., Wang, Y., Li, J., Jiang, X., and Chen, J. (2016). Corrosion and wear behaviors of PVD CrN and CrSiN coatings in seawater. *Trans. Nonferrous Met. Soc. China* 26: 175–184.

Sharma, B.K., Shah, D.V., and Roy, D.R. (2018). Green synthesis of CuO nanoparticles using Azadirachta indica and its antibacterial activity for medicinal applications. *Mater. Res. Express* 5: 095033.

Shaw, A.J. (1994). Defining cell viability and cytotoxicity. *Altern. Lab. Anim.* 22: 124–126.

Shokrani, A., Dhokia, V., and Newman, S.T. (2016). Investigation of the effects of cryogenic machining on surface integrity in CNC end milling of Ti–6Al–4V titanium alloy. *J. Manuf. Process.* 21: 172–179.

Soloviev, M. and Gedanken, A. (2011). Coating a stainless steel plate with silver nanoparticles by the sonochemical method. *Ultrason. Sonochem.* 18: 356–362.

Soofivand, F. and Salavati-Niasari, M. (2013). Novel solvent-less synthesis of CuO nanoparticles by using sublimated precursors. *Mater. Lett.* 106: 83–86.

Sreeram, K.J., Nidhin, M., and Nair, B.U. (2008). Microwave assisted template synthesis of silver nanoparticles. *Bull. Mater. Sci.* 31: 937–942.

Starowicz, M., Stypuła, B., and Banaś, J. (2006). Electrochemical synthesis of silver nanoparticles. *Electrochem. Commun.* 8: 227–230.

Süer, N., Arasoğlu, T., Cankurtaran, H., Okutan, M., Gallei, M., and Eren, T. (2021). Detection of bacteria using antimicrobial polymer derived via ring-opening metathesis (romp) pathway. *Turk. J. Chem.* 45: 986–1003.

Surendhiran, S., Gowthambabu, V., Balamurugan, A., Sudha, M., Kumar, V.S., and Suresh, K.C. (2021). Rapid green synthesis of CuO nanoparticles and evaluation of its photocatalytic and electrochemical corrosion inhibition performance. *Mater. Today Proc.* 47: 1011–1016.

Suresh, K.C. and Balamurugan, A. (2021). Evaluation of structural, optical, and morphological properties of nickel oxide nanoparticles for multi-functional applications. Inorg. *Nano-Metal Chem.* 51: 296–301.

Święch, D., Palumbo, G., Piergies, N., Kollbek, K., Marzec, M., Szkudlarek, A., and Paluszkiewicz, C. (2023). Surface modification of Cu nanoparticles coated commercial titanium in the presence of tryptophan: comprehensive electrochemical and spectroscopic investigations. *Appl. Surf. Sci.* 608: 155138.

Thukkaram, M., Vaidulych, M., Kylián, O., Rigole, P., Aliakbarshirazi, S., Asadian, M., Nikiforov, A., Biederman, H., Coenye, T., Du Laing, G., et al. (2021). Biological activity and antimicrobial property of Cu/aC: H nanocomposites and nanolayered coatings on titanium substrates. *Mater. Sci. Eng., C* 119: 111513.

Ullah, I. (2022a). Activation energy with exothermic/endothermic reaction and Coriolis force effects on magnetized nanomaterials flow through Darcy–Forchheimer porous space with variable features. *Waves Random Complex Medium* 0: 1–14.

Ullah, I. (2022b). Heat transfer enhancement in Marangoni convection and nonlinear radiative flow of gasoline oil conveying Boehmite alumina and aluminum alloy nanoparticles. *Int. Commun. Heat Mass Tran.* 132: 105920.

Usman, M., Ibrahim, N., Shameli, K., Zainuddin, N., and Yunus, W. (2012). Copper nanoparticles mediated by chitosan: synthesis and characterization via chemical methods. *Molecules* 17: 14928–14936.

Van Hengel, I.A.J., Tierolf, M., Valerio, V.P.M., Minneboo, M., Fluit, A.C., Fratila-Apachitei, L.E., Apachitei, I., and Zadpoor, A.A. (2020). Self-defending additively manufactured bone implants bearing silver and copper nanoparticles. *J. Mater. Chem. B* 8: 1589–1602.

Van Meerloo, J., Kaspers, G.J., and Cloos, J. (2011). Cell sensitivity assays: the MTT assay. *Cancer Cell Cult.Method Protoc.*: 237–245, https://doi.org/10.1007/978-1-61779-080-5_20.

Vu, N.B., Truong, N.H., Dang, L.T., Phi, L.T., Ho, N.T.-T., Pham, T.N., Phan, T.P., and Pham, P.V. (2016). In vitro and in vivo biocompatibility of Ti-6Al-4V titanium alloy and UHMWPE polymer for total hip replacement. *Biomed. Res. Ther.* 3: 1–11.

Wang, P., Yuan, Y., Xu, K., Zhong, H., Yang, Y., Jin, S., Yang, K., and Qi, X. (2021). Biological applications of copper-containing materials. *Bioact. Mater.* 6: 916–927.

Wazir, A., Khan, Q.U., Ahmad, N., Ullah, F., Quereshi, I., and Ali, H. (2022). Antimicrobial evaluation and characterization of copper nanoparticles synthesized by the simple chemical method. *Kor. J. Mater. Res.* 32: 80–84.

Xavier, J.R. (2020). Galvanic corrosion of copper/titanium in aircraft structures using a cyclic wet/dry corrosion test in marine environment by EIS and SECM techniques. *SN Appl. Sci.* 2: 1–10.

Xi, D. and Wong, L. (2021). Titanium and implantology: a review in dentistry. *J. Biol. Regul. Hom. Agents* 35: 63–72.

Xia, C., Ma, X., Zhang, X., Li, K., Tan, J., Qiao, Y., and Liu, X. (2020). Enhanced physicochemical and biological properties of C/Cu dual ions implanted medical titanium. *Bioact. Mater.* 5: 377–386.

Xie, H. and Kang, Y.J. (2009). Role of copper in angiogenesis and its medicinal implications. *Curr. Med. Chem.* 16: 1304–1314.

Yağmur, S. and Pul, M. (2021). Investigation of the effect of pre-hole application on machinability in drilling of Ti-6Al-4V titanium alloy. *Uluslararası Muhendislik Arastirma ve Gelistirme Dergisi* 13: 170–177.

Yaprak, E. (2019). *Synthesis, characterization and antimicrobial activity of copper nanoparticles from karabaş lavender (Lavandula stoechas L.) by green synthesis method. master's degree. Thesis*. Atatürk, Turkey, pp. 60.

Yu, L., Jin, G., Ouyang, L., Wang, D., Qiao, Y., and Liu, X. (2016). Antibacterial activity, osteogenic and angiogenic behaviors of copper-bearing titanium synthesized by PIII&D. *J. Mater. Chem. B* 4: 1296–1309.

Zhang, E., Zheng, L., Liu, J., Bai, B., and Liu, C. (2015). Influence of Cu content on the cell biocompatibility of Ti–Cu sintered alloys. *Mater. Sci. Eng., C* 46: 148–157.

Zhang, E., Zhao, X., Hu, J., Wang, R., Fu, S., and Qin, G. (2021). Antibacterial metals and alloys for potential biomedical implants. *Bioact. Mater.* 6: 2569–2612.

Zhang, L.-C. and Chen, L.-Y. (2019). A review on biomedical titanium alloys: recent progress and prospect. *Adv. Eng. Mater.* 21: 1801215.

Zhang, S., Liang, X., Gadd, G.M., and Zhao, Q. (2021). A sol–gel based silver nanoparticle/polytetrafluorethylene (AgNP/PTFE) coating with enhanced antibacterial and anti-corrosive properties. *Appl. Surf. Sci.* 535: 147675.

Zhao, L., Chu, P.K., Zhang, Y., and Wu, Z. (2009). Antibacterial coatings on titanium implants. *J. Biomed. Mater. Res. Part B: Appl. Biomater.* 91: 470–480.

Zhao, L., Wang, H., Huo, K., Cui, L., Zhang, W., Ni, H., Zhang, Y., Wu, Z., and Chu, P.K. (2011). Antibacterial nano-structured titania coating incorporated with silver nanoparticles. *Biomaterials* 32: 5706–5716.

Zhao, Q., Yi, L., Hu, A., Jiang, L., Hong, L., and Dong, J. (2019). Antibacterial and osteogenic activity of a multifunctional microporous coating codoped with Mg, Cu and F on titanium. *J. Mater. Chem. B* 7: 2284–2299.

Zong, M., Bai, L., Liu, Y., Wang, X., Zhang, X., Huang, X., Hang, R., and Tang, B. (2017). Antibacterial ability and angiogenic activity of Cu-Ti-O nanotube arrays. *Mater. Sci. Eng., C* 71: 93–99.